EVALUATION AND COMPARISON OF HELICOPTER SIMULATION MODELS WITH DIFFERENT FIDELITIES

A THESIS SUBMITTED TO
THE GRADUATE SCHOOL OF NATURAL AND APPLIED SCIENCES
OF
MIDDLE EAST TECHNICAL UNIVERSITY

BY

DENİZ YILMAZ

IN PARTIAL FULFILLMENT OF THE REQUIREMENTS
FOR
THE DEGREE OF MASTER OF SCIENCE
IN
AEROSPACE ENGINEERING

JULY 2008

Approval of the thesis:

EVALUATION AND COMPARISON OF HELICOPTER SIMULATION MODELS WITH DIFFERENT FIDELITIES

submitted by **DENİZ YILMAZ** in partial fulfillment of the requirements for the degree of **Master of Science in Aerospace Engineering Department, Middle East Technical University** by,

Prof. Dr. Canan Özgen
Dean, Graduate School of **Natural and Applied Sciences** _____

Prof. Dr. İsmail H. Tuncer
Head of Department, **Aerospace Engineering** _____

Dr. İlkay Yavrucuk
Supervisor, **Aerospace Engineering Dept., METU** _____

Examining Committee Members:

Prof. Dr. Cahit Çıray
Aerospace Engineering Dept., METU _____

Dr. İlkay Yavrucuk
Aerospace Engineering Dept., METU _____

Prof. Dr. Ozan Tekinalp
Aerospace Engineering Dept., METU _____

Assist. Prof. Dr. Oğuz Uzol
Aerospace Engineering Dept., METU _____

Assist. Prof. Dr. Nilay Sezer Uzol
Mechanical Engineering Dept.,
TOBB University of Economics and Technology _____

Date: _____

I hereby declare that all information in this document has been obtained and presented in accordance with academic rules and ethical conduct. I also declare that, as required by these rules and conduct, I have fully cited and referenced all material and results that are not original to this work.

Name, Last Name: DENİZ YILMAZ

Signature :

ABSTRACT

EVALUATION AND COMPARISON OF HELICOPTER SIMULATION MODELS WITH DIFFERENT FIDELITIES

Yılmaz, Deniz

M.S., Department of Aerospace Engineering

Supervisor : Dr. İlkay Yavrucuk

July 2008, 76 pages

This thesis concerns the development, evaluation, comparison and testing of a UH-1H helicopter simulation model with various fidelity levels. In particular, the well known minimum complexity simulation model is updated with various higher fidelity simulation components, such as the Peters-He inflow model, horizontal tail contribution, improved tail rotor model, control mapping, ground effect, fuselage interactions, ground reactions etc. Results are compared with available flight test data. The dynamic model is integrated into the open source simulation environment called Flight Gear. Finally, the model is cross-checked through evaluations using test pilots.

Keywords: helicopter, simulation, fidelity, mathematical modeling

ÖZ

GERÇEKÇİLİĞİ DEĞİŞKEN HELİKOPTER MODELLERİNİN DEĞERLENDİRİLMESİ VE KARŞILAŞTIRILMASI

Yılmaz, Deniz
Yüksek Lisans, Havacılık ve Uzay Mühendisliği Bölümü
Tez Yöneticisi : Dr. İlkay Yavrucuk

Temmuz 2008, 76 sayfa

Bu tez değişik gerçekçilik seviyeleri olan UH-1H helikopter simülasyon modellerinin geliştirilmesini, testini ve karşılaştırılmasını içerir. Literatürde iyi bilinen ”minimum complexity” simulasyon modelinin kontrol dağıtımı, yatay kanatcık aerodinamiği, rotor iç akışı, gövde, yer etkileşimi gibi yeni birimler ile gerçeklik seviyesi artırıldı. Sonuçlar uçuş test verisi ile karşılaştırıldı ve test pilotları tarafından simulasyon ortamında denendi.

Anahtar Kelimeler: helikopter, simülasyon, gerçekçilik, matematiksel modelleme

To my family

ACKNOWLEDGMENTS

I would like to express my sincere gratitude to Dr. İlkay Yavrucuk who supervised in all steps of this work and provided the necessary resources of his knowledge and experience. His energy, support and guidance helped me to complete this work.

I would like to thank Prof. Dr. Cahit Çıray for setting the first light about helicopters in my mind during my undergraduate years. Also, many thanks to Assoc. Prof. Dr. Serkan Özgen for encouraging me to start my master thesis about helicopter simulation. Special thanks to Prof. Dr. Ozan Tekinalp and Assist. Prof. Dr. Oğuz Uzol for their assistance and suggestions. I wish to state my thanks to the Teoman Özmen, who has never turned down my specific requests about UH-1H helicopters and simulators located in helicopter maintenance center military base.

I wish to state may endless thanks to Onur Tarımcı and Şevket Eser Kubalı. I probably would not be able to finish my thesis without their help about coding and integration to simulation environment. I would like to thank Özlem Ceyhan and Adnan Ceyhan for sharing my whole thesis progress. I appreciate the useful discussions we had with Volkan Kargın and Hilal Erçin. I can not forget the assistance of Tolga Yapıcı, Tahir Turgut and Emre Altuntaş about latex formating. I also would like to thank Gürsu Taşar, Alper Ezertaş and Gökhan Ahmet for always being on my side during the thesis. Thanks to Dr. Mustafa Kaya for his supports too. I would like to thank all my friends working in the same laboratory; Burcu Akın, Tuba Çiğdem Elmas, Sinem Işık, Zeynep Çakır and Onur Tarımcı for supporting me whenever I needed. Also many thanks to my friends, Burcu Çakın Erdoğan and Buşra Akay who had been far away but close enough to share my thesis progress. Special thanks to all aerospace engineering department staff for their kind responses.

Finally, I would like to express my deepest thanks to my parents for their endless support throughout my life. Also, this thesis is supported by the 106M069 project of The Scientific and Technological Research Council of Turkey (TUBITAK).

TABLE OF CONTENTS

LIST OF TABLES

TABLES

LIST OF FIGURES

FIGURES

LIST OF ABBREVIATIONS

ϕ	Roll angle
θ	Pitch angle
ψ	Yaw angle
C_T	Thrust coefficient
ψ	Azimuth angle
$\hat{r}$	Radial section
$\hat{t}$	Non dimensional time
$\hat{u}(\hat{r}, \psi, \hat{t})$	Induced flow distribution
$\phi_j^r(\hat{r})$	Radial expansion function
(M)	Apparent mass matrix
(L)	Inflow coefficient matrix
$()^*$	Derivation w.r.t non dimensional time
χ	Wake skew angle
V	Flow parameters matrix
V_T	Total flow parameter
μ	Advance ratio
λ	Inflow ratio
τ	Pressure coefficient
p	Body roll rate
q	Body pitch rate
r	Body yaw rate
B_{1s}	Longitudinal cyclic control
A_{1s}	Lateral cyclic control
K_B	Stabilizer bar mechanical mixing ratio gain
τ_B	Mechanical damping constant
Re	Reynold's number
μ_d	Dynamic viscosity of the air
$C_{d,0}$	Drag coefficient of airfoil
C_L	Lift coefficient of horizontal stabilizer
AR	Aspect Ratio
e	Span Efficiency
C_D	Drag coefficient of horizontal stabilizer
$()_{gear}$	Landing gear
$()_{body}$	Body axis
c	Damping coefficient of landing gears
$\dot{x}_c$	Compression rate of landing gears
k	Spring coefficient of landing gears
x_c	Landing gear compression length
F_{gear}	Force on landing gear
N	Normal force
f_d	Dynamic coefficient of friction of skid
f_s	Static coefficient of friction of skid
β_f	Exponential coefficient of decay
V_{rel}	Relative velocity of the surface
F_{fx}	Forward friction force
F_{fy}	Sideward friction force
F_{lgX}	Friction force in x-axis of body at center of gravity
F_{lgY}	Friction force in y-axis of body at center of gravity
F_{lgZ}	Friction force in z-axis of body at center of gravity
$()_{SL}$	Sea level conditions
$()_{ISA}$	Desired level conditions
h	Altitude
ρ	Air density
T	Thrust
$()_{IGE}$	In ground effect
$()_{OGE}$	Out of ground effect
R	Main rotor radius
Z	Altitude of hub
V_f	Forward velocity
V_i	Induced velocity

K	Ground effect constant
$\dot{()}$	Derivation w.r.t time
L	Roll moment
M	Pitch moment
N	Yaw moment
I_X	Inertia in body x-axis
I_Y	Inertia in body y-axis
I_Z	Inertia in body z-axis
I_{XZ}	Inertia on body x-z plane
U	Velocity in body x-axis
V	Velocity in body y-axis
W	Velocity in body z-axis
$\dot{x_e}$	Velocity in earth x-axis
$\dot{y_e}$	Velocity in earth y-axis
$\dot{z_e}$	Velocity in earth z-axis
δ_a	Lateral control
δ_e	Longitudinal control
δ_p	Pedal control
δ_c	Collective control
B	Control matrix
A_1, A_2	Stability matrices
g	Gravity of earth
U_1, U_2, U_3	Linear controller outputs
A_D	Total acceleration command
$L_{VB}(\phi, \theta, \psi)$	Transformation matrix from body fixed to earth fixed fame
$()_D$	Commands
$()_i$	Initials
F_x	Force in body x-axis
F_y	Force in body y-axis
F_z	Force in body z-axis
m	Mass of the helicopter
$\ddot{X}$	Acceleration in earth x-axis
$\ddot{Y}$	Acceleration in earth y-axis
$\ddot{Z}$	Acceleration in earth z-axis

CHAPTER 1

INTRODUCTION

Since the first production of helicopters, the flight envelope of rotorcraft has been expanded and maneuvers became more complex. Demands increased due to unique characteristics of helicopters like hovering, vertical take off and landing. New requirements increased the workload of the helicopter by means of accomplishing the recent missions and this also leads to excessive pilot workload. Hence, helicopter training became more demanding.

Many widely used helicopters have their roots in older designs. Yet, any technological improvement in aviation technology is applied to older platforms almost instantaneously. Hence, helicopter platforms are being modified with an increasing trend. Modifying the helicopter systems results in new testing procedures and training exercises.

Pilot training is a difficult and dangerous process, when actual aircraft is used, mainly because helicopters are unstable air vehicles at low speeds and require complex controls. During the training period, not only standard flight missions but also emergency situations with risky recovery applications are practiced. The International Helicopter Safety Team's Joint Helicopter Safety Analysis Team (JHSAT) has concluded that more helicopter accidents occur during pilot training than in any other area of operation [25]. Also, World Aircraft Accident Summary (WAAS) reports that the greatest cause for accidents is pilot loss of control [27] and addresses the importance of pilot training.

Helicopter simulators are being used to support the training period in a much safer and more economical way. Also, JHSAT reports that helicopter pilots should be given the advantage of scenario-based training, which they can only get from simulation. In addition, a simulator enables successful malfunction training, flight repositioning to repeat exercises quickly, and

recording and playback to enable debriefing [25].

Simulators are generally composed of 5 main parts; computers for real time mathematical models with various fidelity levels, pilot control mechanisms, ground station computers for instructors, visualization systems and motion platforms. Depending on their accuracy to mimic a real helicopter, -including the dynamics, avionics, cockpit and motion- several levels of simulators exist: Synthetic Training Devices (STD), Flight Navigation and Procedure Trainers (FNPT) to Level D simulators with full motion platform, high precision visualization, very high fidelity helicopter models and real time synchronized multi mission capability with other simulators.

Before the technological improvements in computers, real time helicopter modeling had always been a big challenge due to the lack of high speed computer processors and supporting hardware. One of the first real time helicopter simulation model applications can be found in reference [30] in which a Wessex simulator was described with the technology of 1970's. Although real helicopter avionics and controls were used on a motion platform, the mathematical dynamic simulation model embedded in the simulator was inevitably simple due to lack of computing power. In the following years, in 1977, a more complicated simulation model for the UH-1H is developed for piloted simulation purposes [2]. This approach uses uniform inflow over the entire tip path plane, simple expressions for contributions of the tail rotor, fuselage and empennage. Also, it contains quasi-static main rotor representation, no interaction of components and ignores the main rotor shaft tilt throughout the calculations. In addition to these assumptions, one frail side of the simulation model is that constants are introduced to match the flight data throughout the calculations for specific flight conditions and these constants must be adjusted for different flight regimes. As indicated in the reference, while adjusting the coefficients for hover, divergence was observed for 60 knots flight condition. Moreover, different coefficients for various limiting conditions caused the model to experience difficulty in trim. On the other hand, most of the specifications of the UH-1H helicopter is obtained from this reference since detailed study was carried out for pilot in the loop simulation. Two years later, Robert T.N. Chen published a NASA technical Memorandum paper which is focused on the helicopter main rotor dynamics [32]. Although complicated sets of equations are developed for main rotor calculations including flapping hinge restraint, effective hinge offset and pitch-flap coupling, some of the model assumptions prevented the usage of the mathematical model through entire flight envelope. In the following year, Robert

T.N. Chen extended the research by containing teetering and non-teetering configurations with more complicated sets of equations [33]. But absence of powerful computing capability of the computers prevented the application of the concept of real time simulations and reduced model sets were introduced. In 1982, Ames Research Center published a scientific paper about a simulation model application for piloted simulation [34]. The application described is an extended version of reference [32] but still limited for specific flight regimes because of the assumptions containing basic momentum theory with uniform inflow, simple strip theory, absence of reversed flow region and tip loss effect. In 1986, Robert Hefley and Marc Mnich from the NASA Ames Research Center published a real time mathematical simulation model, which reflected the idea of developing a method to cover the whole flight regimes with minimum complicated calculations, known as the minimum complexity model. This model is chosen to be the initial model in this research and it will be described in details in the following chapters.

Parallel to the developments in general helicopter dynamics, improvements in the main rotor inflow distribution models -one of the most critical components in helicopter modeling- were also noticed. The main obstacle for implementing the complicated flow characteristics has been the limitation in computing power during real time applications. Advanced computational fluid dynamics (CFD) software are able to solve the flow properties but with considerable computation time even with advanced computing hardware. Early on the inflow distribution was mainly solved by the use of Classical Momentum Theory, Glauert's Theory and their modifications for different flight conditions [5], [6], [7], [35]. Interests had been focusing on non-uniform inflow modeling, which predicted the main rotor calculations in a more accurate way. The Pitt-Peters inflow model [40], [41] was one of the milestones of dynamic non-uniform inflow models. A detailed historical development of non-uniform inflow models is listed in the survey of Chen [42]. Takahashi [46] from the NASA Ames Research Center reported a flight dynamics mathematical model of a single rotor helicopter, which benefits from the Pitt-Peters dynamic inflow model. Although the model shows great correlation with the UH-60A Black Hawk helicopter test data, linearization and simplified blade loading calculations doesn't allow its validity for the entire flight envelope in real time simulation application. Later, another method was published; the finite state rotor induced flow model with a set of closed-form, first order, ordinary differential equations in time defining a finite number of modal inflow states with blade lift as the forcing function [43], [44]. This model is also

known as the Peters-He generalized dynamic wake method, which is described in first section of the following chapter. Most of the state-of-the-art helicopter simulations use this method for inflow calculations. For example the popular simulation code FLIGHTLAB (Advanced Rotorcraft Technoloy) uses three state Peters-He inflow model with empirical corrections for vortex ring state, similarly COPTER (Bell Helicopter) and ONERA-DFVLR (European Community) [50] use this inflow model. This thesis also makes use of this computationally efficient Peters-He inflow model.

Parallel processor implementations were also used for rotorcraft simulation for the handling of the complex calculations [31]. In 1996, Krothapalli, Peters and Prasad introduced a new method [47] composed of momentum, actuator disk and vortex theory. Hover case validations showed that models differ in predicting inflow distributions due to hub rotations by a factor of three. Finite state inflow models had various applications like the implementation of ground effect for dynamic ground [48], which impedes the imaging method of vortex theory.

In 2000, a free wake inflow implementation to a helicopter mathematical model was performed [49], which is strictly valid only in steady-state conditions and can not be rigorously used in a time marching procedure. Morillo and Peters [50] improved the general dynamic wake method for obtaining all three velocity components in axial flow, which is hierarchical to the Peters-He model but also has ability to treat induced flow components anywhere above or below the rotor disk [53], and searched the numerical stability of the methodology. In 2002, constants from vortex tube analysis were integrated to Peters-He inflow model [51], which is a modification to the model to represent the transient effects by distorting wakes. As a result, good off-axis response characteristic matching was obtained. In 2003, Houston and Brown [52] reported a study about the comparison of the Peters-He and vortex tube analysis and concluded that the 5 state Peters-He inflow model is adequate for most of the autorotation regime, whereas improvements are needed for steep and low speed descent cases. Zhao et. al. [54] reported a detailed anaylsis of dynamic wake distortion and their applications to the Peters-He inflow model. With the recent improvements in computing power, complicated free-wake models (GENHEL and CHARM) are being used in real time helicopter simulation applications [55]. Although considerable achievements are obtained for high amplitude controls, free wake models still need optimum constraint selections like blade loading resolution and refresh rate of induced velocity field creation. Moreover, it is concluded that finite state inflow models show good correlation around small amplitudes on axis responses when com-

pared to advanced free-wake baseline models. In 2006, C. Chen researched inflow models during descent flight [56], especially the vortex ring state (VRS). Also, Some of the fidelity researches and methods are listed in references [3], [6]. A recent survey about inflow and wake models is listed in reference [57].

Generally, dynamic mathematical simulation models are coded computer languages like Fortran or C++ due to their fast computing abilities. C++ has been used in flight simulation applications for many years due to it's ability of being easily reconfigurable, object oriented programming skills like polymorphism, inheritance, encapsulation and abstraction and integrated development environments (IDEs), easy adaptation to various hardware configurations [26]. In this work the codes were written in C++ and the open source simulation environment called FlightGear is used to visualize the dynamics. Although FlightGear can interact with codes written in various computer languages such as Matlab-Simulink and Fortran, internal implementation of the C++ generated helicopter model resulted in more flexible testing and debugging capabilities.

A common approach to generate a simple model of a helicopter is to start with the minimum complexity model. However, when applied to the UH-1H helicopter, it is observed that this approach is not enough. On the other hand, advanced models could be built with high modeling fidelity. This thesis targets a model that is just enough to model the UH-1H helicopter close to available through flight test data without using the most advanced high fidelity simulation components such as flow interactions, etc. to be used in real time simulation. Therefore it is targeted to include only the effects that are absolutely necessary to avoid the need to excessive computing power. As a result, this thesis focuses on the real time mathematical dynamic helicopter model development with various simulation fidelity levels and integration of the models into a representative simulation environment. Therefore, new mathematical models of UH-1H with different fidelity levels will be used for simulator applications and simulation purposes. Simulation fidelity is considered as the combination of objective fidelity, which is defined as similarity of the simulation model to flight test data, and perceptual fidelity, which is defined as the subjective judgment of pilots on simulation model [58],[59]. The chosen helicopter to simulate is the UH-1H (Huey), which has published flight tests and specifications data. Moreover, there were experienced UH-1H test pilots for simulation evaluations.

This thesis is organized as follows: Chapter 2 describes the component built up method used

for simulating the UH-1H helicopter. Component calculations are investigated and developed separately through the sub sections. Minimum complexity and updated simulation models are introduced and described. Chapter 3 addressees the trimmer, which is designed for finding trim conditions of simulation models. In chapter 4, trim values , dynamic responses of simulation models are verified with existing flight test data. Moreover, integration to simulation environment and conclusions of performed pilot evaluations are listed. Finally, chapter 5 presents conclusions and recommendations for future work.

CHAPTER 2

MATHEMATICAL MODELING

The mathematical modeling of the UH-1H is accomplished by the component build up method. Forces and moments of components are carried to the center of gravity of the helicopter for calculating the rotational and translational state derivatives and instantaneous states of the simulated helicopter. During the calculations, contributions of altitude, ground effect, landing gears and ground reactions are included. There are two versions of simulation models throughout the research; the minimum complexity and the so-called "updated model", a model with updates to the minimum complexity model.

In reference [1], an example helicopter is modeled for pilot training using as simple components as possible. The idea is to include only the effects that a pilot in simulation would feel; hence the name minimum complexity. Here the main rotor flapping is calculated by a first order flapping dynamics assumption. The calculations of induced velocities of the both main and tail rotors are iterative methods based on classic momentum theory and Glauert theory [6], [5], [7], [1]. Quadratic lift coefficients are used to model the aerodynamic forces and moments on the various components of the helicopter, including horizontal stabilizer, vertical tail and fuselage. Main rotor inflow effects onto those components are also included. Finally, performance parameters such as the profile power of the main rotor, power required for climbing and parasite power are calculated separately. In this thesis, the mathematical methodology is kept the same but the geometrical properties of the original code is modified for the UH-1H and finally, a minimum complexity mathematical helicopter simulation of the UH-1H is obtained. The minimum complexity model is set as the baseline model.

Next, modifications are made to the baseline model and an updated simulation model is developed to obtain a more detailed simulation model of the UH-1H. Helicopter specific compo-

nents such as a stabilizer bar, a horizontal tail with varying incidence angle according to pilot longitudinal cyclic were included. Calculations of some components are extended to involve more complex effects like inflow distribution on main rotor. Each modification is explained separately in the following subsections. A general schema of the simulation model is shown in figure 2.1.

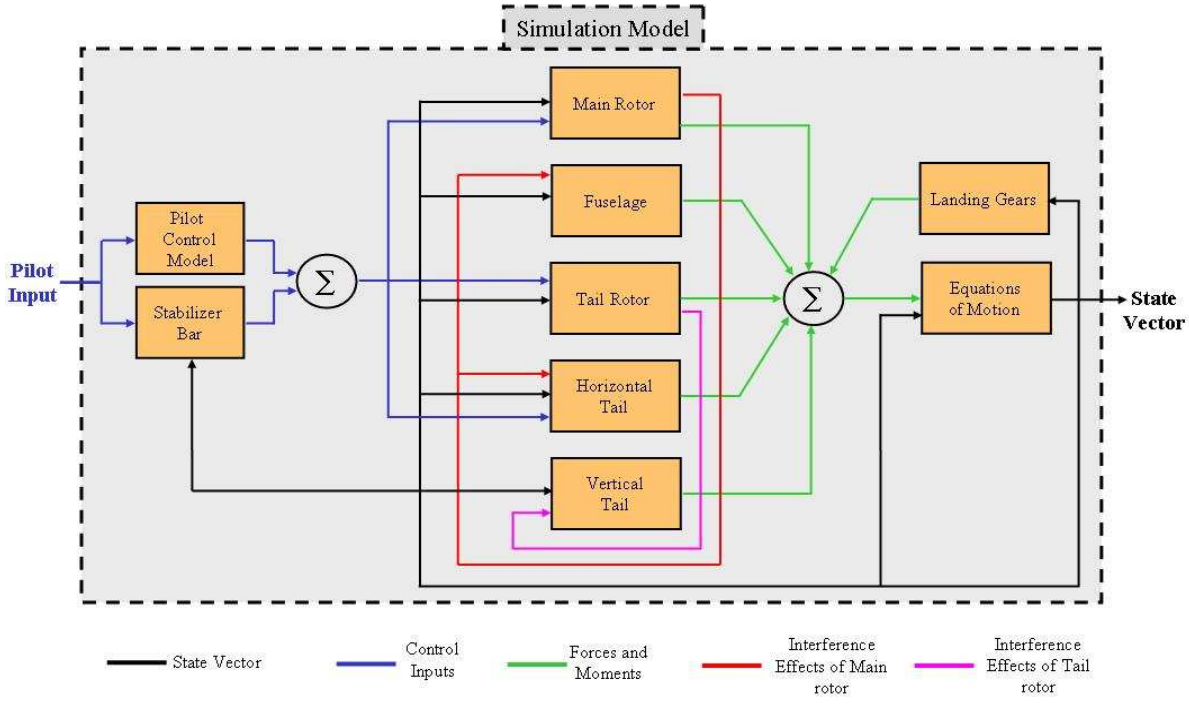

Figure 2.1: A general schema of simulation model algorithm structure.

Both the baseline model and the updated model share the following commonly used assumptions and approaches:

- An ideal engine assumption is made, i.e. the engine is always capable of providing enough power and therefore constant rotational speed of the main rotor and tail rotor.
- Main rotor blade is a rigid body and is not effected by aeroelastic forces and moments.
- Weather conditions are assumed to be steady without any gust, turbulence and wind.
- Weight and center of gravity of models are fixed throughout the simulation.

- Special modifications to cover autorotation and vortex ring state regimes are not implemented into the simulation models.

- Off-axis response modification is not included in the simulation models.

2.1 Main Rotor Modeling

The main rotor has the most dominant role on the helicopter dynamics since directional controlling, propulsive and lifting forces are mostly generated by the main rotor. Thus, modeling the main rotor is a challenging process. There has been the use of highly sophisticated CFD methods, experimental procedures and multidisciplinary analysis to understand the behavior of the main rotor dynamics, including inflow distributions and coupled flapping, real time pilot in the loop helicopter simulations. It is computationally very demanding to include all aeroelastic effects, complex unsteady inflow characteristics with detailed interaction of lifting surfaces and complicated vibration effects in real time. In the future, it might be possible to include more sophisticated models in real time simulation systems.

Both the minimum complexity and the updated simulation models use first order flapping equations, which are accurate enough for the pilot in the loop real time applications. The basis of the model belongs to Glauert [35] and Lock [36].Then, in reference [1] the equations were simplified by integrating the flapping calculations [33] for real time applications. First order flapping equations result in a tip path plane (TPP) lag affecting the main rotor thrust vector orientation and instantaneous control changes. Detailed information about flapping calculations is present in diploma thesis of Munzinger [37]. In reference [38], a work is done to analyze the effects that simulator tolerances may have on the level of fidelity used in helicopter mathematical models and it is concluded that for a teetering rotor complicated flapping dynamics are hardly noticeable.

One of the main difference between minimum complexity and the updated model is the calculations of main rotor thrust and inflow. Minimum complexity uses uniform flow distribution and calculates thrust based on momentum theory. On the other hand, the updated model includes Peters-He inflow distribution model with a blade element approach for the main rotor thrust calculation. Considering the real time performance, blade is considered as three sections during this research. Since state of the art simulation applications contain 5 sections of

blades for the real time simulation of the mathematical models [28] , a three section configuration was thought to be a reasonable choice for this initial work.

The Peters-He inflow model, which is also known as the generalized dynamic wake (GDW) model, is an extension of the often used Pitt-Peters model. The GDW model is originated from acceleration potential flow calculations with a skewed cylindrical wake assumption [43]. Although rotor disk is assumed as a flat plate in the GDW model, individual elements of rotor blades is taken into account according to their azimuth and radial position. Aerodynamic forces are explicitly included in the GDW model, which provides the flexibility of choosing linear or nonlinear blade element calculations.

GDW model has some advantages on blade element momentum (BEM) models such that it follows for a more general distribution of pressure across a rotor plane, inherent modeling of tip loss and excluding iterative methods. However standard GDW also has limitations like instability during low speed turbulent wake and vortex ring states, not including wake rotation and assuming rotor plane as flat disk which lacks the aeroelastic modeling. Derivations of the GDW is determined in references [43], [44] and [45]. The resultant methodology is summarized next.

Induced flow distribution, which depends on radial sections, azimuth of the blade and time, can be represented by the following equation.

$$\hat{u}(\hat{r},\psi,\hat{t}) = \sum_{r=0}^{N} \sum_{j=r+1,r+3,\ldots}^{2S_r+r-1} \phi_j^r(\bar{r}) \left[\alpha_j^r(\hat{t})\cos(r\psi) + \beta_j^r(\hat{t})\sin(r\psi)\right] \tag{2.1}$$

where $\bar{r}$ is the non dimensional blade coordinate ($\bar{r}$=r/R), ψ is the azimuth of the blade, $\hat{t}$ is the non dimensional time ($\hat{t}$=Ωt), N is the highest harmonic in the azimuthal direction, S_r is the number of radial shape functions, $\phi_j^r(\bar{r})$ is the radial expansion function, $\alpha_j^r(\hat{t})$ and $\beta_j^r(\hat{t})$ are the inflow coefficients. Radial expansion function has the following form,

$$\phi_j^r(\hat{r}) = \sqrt{(2j+1)H_j^r}\Sigma\hat{r}^q \frac{(-1)^{\frac{q-r}{2}}(j+q)!!}{(q-r)!!(q+r)!!(j-q-1)!!} \tag{2.2}$$

$$H_j^r = \frac{(j+r-1)!!(j-r-1)!!}{(j+r)!!(j-r)!!} \tag{2.3}$$

n!! is a double factorial, defined as,

$$n!! \equiv \begin{cases} n(n-2)(n-4)\cdots 3\ 1, & \text{if } n = \text{even} \\ n(n-2)(n-4)\cdots 4\ 2, & \text{if } n = \text{odd} \end{cases} \tag{2.4}$$

Inflow coefficients, which are the states of the GDW, are related with pressure coefficients τ's according to the following matrix formation;

$$[M^c] \begin{Bmatrix} \vdots \\ \{\alpha_j^r\} \\ \vdots \end{Bmatrix}^* + \left[\tilde{L}^c\right]^{-1} \left[\hat{V}^c\right] \begin{Bmatrix} \vdots \\ \{\alpha_j^r\} \\ \vdots \end{Bmatrix} = \frac{1}{2} \begin{Bmatrix} \vdots \\ \{\tau_n^{mc}\} \\ \vdots \end{Bmatrix} \tag{2.5}$$

$$[M^s] \begin{Bmatrix} \vdots \\ \{\beta_j^r\} \\ \vdots \end{Bmatrix}^* + \left[\tilde{L}^s\right]^{-1} \left[\hat{V}^s\right] \begin{Bmatrix} \vdots \\ \{\beta_j^r\} \\ \vdots \end{Bmatrix} = \frac{1}{2} \begin{Bmatrix} \vdots \\ \{\tau_n^{ms}\} \\ \vdots \end{Bmatrix} \tag{2.6}$$

where sine and cosine components of apparent mass matrix M, which are M^s and M^c respectively, are identical except the cosine matrix operator has m=0,1,2,3,... whereas sine matrix operator has m=1,2,3,.... The apparent mass matrix is formulated as follows;

$$[M] = \begin{Bmatrix} \ddots & & \\ & K_n^m & \\ & & \ddots \end{Bmatrix} \tag{2.7}$$

where

$$K_n^m = \frac{2}{\pi} H_n^m = \frac{2}{\pi} \frac{(n+m-1)!!(n-m-1)!!}{(n+m)!!(n-m)!!} \tag{2.8}$$

L^c and L^s are the induced flow influence coefficient matrices, which are defined by the following set of equations ;

$$[L^c]^{-1} = \left[\tilde{L}^c\right]^{-1} \left[\hat{V}^c\right] \tag{2.9}$$

$$[L^s]^{-1} = \left[\tilde{L}^s\right]^{-1} \left[\hat{V}^s\right] \tag{2.10}$$

Sine and cosine components of L operator, which is also known as inflow gain matrix, contain matrices that depend on wake skew angle χ, and they can be expressed as ;

$$\left[\tilde{L}_{jn}^{om}\right]^{c} = X^{m}\left[L_{jn}^{om}\right] \tag{2.11}$$

$$\left[\tilde{L}_{jn}^{rm}\right]^{c} = \left[X^{|m-r|} + (-1)^{l}X^{|m+r|}\right]\left[L_{jn}^{rm}\right] \tag{2.12}$$

$$\left[\tilde{L}_{jn}^{rm}\right]^{s} = \left[X^{|m-r|} - (-1)^{l}X^{|m+r|}\right]\left[L_{jn}^{rm}\right] \tag{2.13}$$

with

$$l = \min(r, m) \tag{2.14}$$

$$X = \tan\left|\frac{\chi}{2}\right| = \frac{\mu}{V_T + |\lambda|}, \quad (0 \le \chi \le \pi/2) \tag{2.15}$$

$$\Gamma_{jn}^{rm} = \frac{(-1)^{\frac{n+j-2r}{2}}}{2\sqrt{H_n^m H_j^r}} \frac{2\sqrt{(2n+1)(2j+1)}}{(j+n)(j+n+2)\left[(j-n)^2-1\right]}, \quad for\ r+m = even \tag{2.16}$$

$$\Gamma_{jn}^{rm} = \frac{\pi}{2\sqrt{H_n^m H_j^r}} \frac{sign(r-m)}{2\sqrt{(2n+1)(2j+1)}}, \quad for\ r+m = odd\ and\ |j-n| = 1 \tag{2.17}$$

$$\Gamma_{jn}^{rm} = 0, \quad for\ r+m = odd\ and\ |j-n| \neq 1 \tag{2.18}$$

Sine and cosine components of flow parameters matrix, $\hat{V}$, are almost identical with the exception of m = 0 as follows;

$$\left[\hat{V}^{c}\right] = \left\{ \begin{array}{ccc} \ddots & & \\ & \hat{V}_n^m & \\ & & \ddots \end{array} \right\} for\ m = 0, 1, 2, 3, \ldots \tag{2.19}$$

$$\left[\hat{V}^s\right] = \left\{ \begin{array}{ccc} \ddots & & \\ & \hat{V}_n^m & \\ & & \ddots \end{array} \right\} for\ m = 1, 2, 3, \ldots \tag{2.20}$$

where

$$\hat{V}_1^0 = V_T\ for\ (m, n) = (0, 1) \tag{2.21}$$

$$\hat{V}_n^m = V\ for\ (m, n) \neq (0, 1) \tag{2.22}$$

Flow parameters matrix, V, is defined as ;

$$V = \frac{\mu^2 + (\lambda + \lambda_m)\,\lambda}{\sqrt{\mu^2 + \lambda^2}} \tag{2.23}$$

and the total flow parameter

$$V_T = \sqrt{\mu^2 + \lambda^2} \tag{2.24}$$

where μ is the advance ratio, λ and λ_m are the inflow ratios calculated as the following equations;

$$\lambda = \lambda_m + \lambda_f \tag{2.25}$$

where λ_f is the normal component of the helicopter forward velocity and λ_m is the unsteady inflow ratio calculated as follows;

$$\lambda_m = \sqrt{3}\alpha_1^0 \tag{2.26}$$

Peters-He inflow model is a perturbation method but with some modifications, a complete nonlinear version is obtained as in references [43], [44] by replacing V with $\sqrt{\mu^2 + \lambda^2}$ just for the first row of $[L^c]^{-1}$, treating all quantities as total rather than perturbation and using the unsteady value of λ_m.

Pressure coefficient harmonics are obtained by the following equation set;

$$\tau_n^{mc} = \frac{1}{\pi\rho\Omega^2 R^4} \sum_{q=1}^{B} \left[\sum_{i=1}^{N_E} L_i^q \phi_n^m (\hat{r}_i) \right] \cos m\psi \tag{2.27}$$

$$\tau_n^{ms} = \frac{1}{\pi\rho\Omega^2 R^4} \sum_{q=1}^{B} \left[\sum_{i=1}^{N_E} L_i^q \phi_n^m (\hat{r}_i) \right] \sin m\psi \tag{2.28}$$

$$\tau_n^{0c} = \frac{1}{\pi\rho\Omega^2 R^4} \sum_{q=1}^{B} \left[\sum_{i=1}^{N_E} L_i^q \phi_n^0 (\hat{r}_i) \right] \tag{2.29}$$

where L_i^q is the sectional lift of the q^th blade and i^th section. Throughout the calculations, normalized element thrust is found as;

$$normalized\ element\ sectional\ lift = \frac{L_i^q}{\rho A(\Omega R)} \tag{2.30}$$

For the blade sectional lift and drag calculations, instead of a linear lift curve assumptions, which neglects reverse flow and high angle of attacks that leads to stalling cases, a more comprehensive blade calculation method is followed. An empirical study of some airfoils is listed in reference [14] for various Reynolds numbers and data is fitted to curves. The methodology is described in details in section 2.4. Although UH-1H has a NACA0012 airfoil in the main and tail rotors, generated curve fitted dynamic libraries are for NACA0015, which is the airfoil type of UH-1. During the computation of sectional forces, induced velocity is taken into account and this feedback couples the GDW equations, which results in including unsteady effects. Moreover, GDW comprises the tip loss effects implicitly. Sample distributions of main rotor local inflow, thrust coefficient and angle of attack are presented in Appendix B.

Control mapping between the pilot controls and the swashplate inputs is provided using references [2] and [8].

During the trimming process, rotor and inflow states are trimmed in addition to helicopter states. One revolution of each blade is calculated by segmenting the blade rotation to 16 equal azimuth angles (22.5 degrees). Although instantaneous thrust, blade drag and inflow distribution are available, in each time step, calculations are performed using azimuth averaged values of the blades since the overall responses were almost identical. The following graphs are plotted to show the responses of the updated simulation models, which include

the Peters-He inflow, with instantaneous and azimuth averaged inflow distributions. After a trimmed flight of one second, step pilot inputs to all channels are applied simultaneously to models , "Inst. Inf. Mod." refers to the model with instantaneous thrust, torque and induced flow calculations, whereas " Avr. Inf. Mod." refers to model with azimuth averaged calculations of the same parameters.

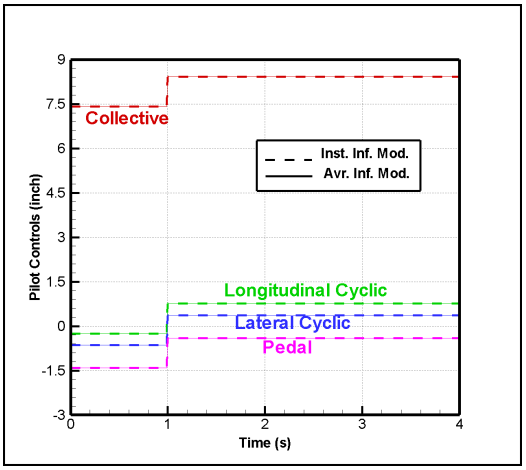

Figure 2.2: Simultaneously applied pilot control inputs to updated simulation models with instantaneous and azimuth averaged inflow calculations.

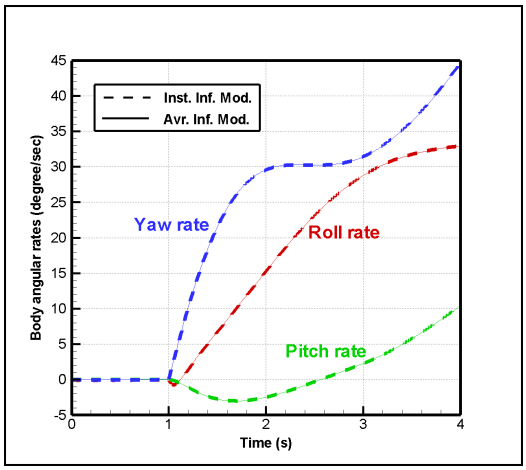

Figure 2.3: Body angular rate responses of updated simulation models with instantaneous and azimuth averaged inflow calculations.

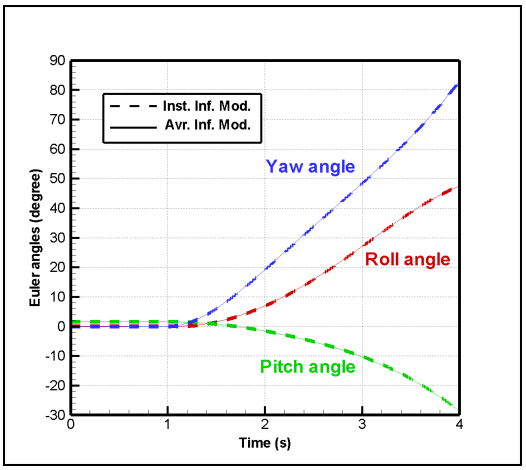

Figure 2.4: Euler angle responses of updated simulation models with instantaneous and azimuth averaged inflow calculations.

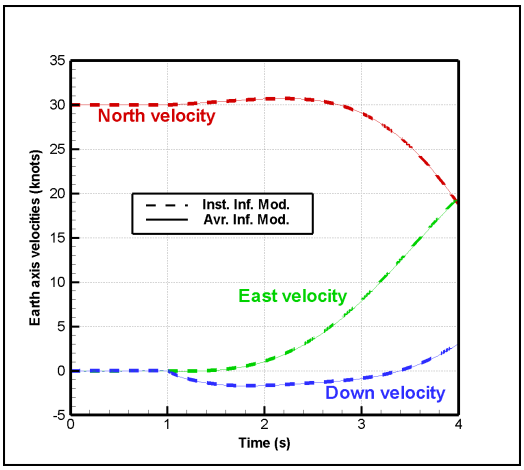

Figure 2.5: Earth axis velocity responses of updated simulation models with instantaneous and azimuth averaged inflow calculations.

It is seen from figures 2.2 and 2.3 that trimmed pilot controls and body angular rate responses of models with instantaneous and azimuth averaged inflow calculations are almost identical. Considering the pilot control inputs, which are applied to whole channels simultaneously, exact similarity of resultant responses, as in figures 2.4 and 2.5, lead to the conclusion that inflow calculations can be chosen according to the application in hand. In this thesis, azimuth averaged calculations are chosen due to their ease of graphical representation and comparison. In figure 2.5, North-East -Down navigation frame with flat earth assumption is used and initially with zero yaw angle, Euler transformation implies the forward flight condition.

2.2 Stabilizer Bar Modeling

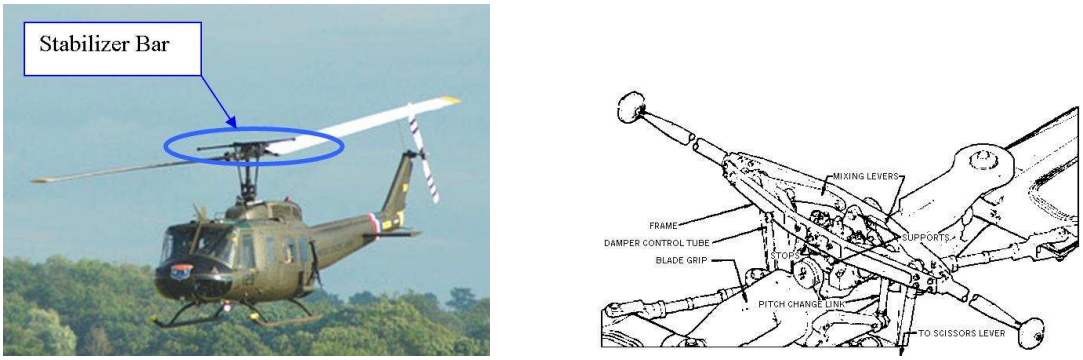

Figure 2.6: Stabilizer bar on UH-1H helicopter.

As seen in figure 2.6 [12],[13], UH-1H has a shaft-mounted stabilizer bar on the main rotor mechanism.

A stabilizer bar is a mechanical augmentation device which increases the damping of the system. Hence, the stabilizer bar effects the stability and control characteristics of the helicopter. The pitch rate is fed back to the longitudinal cyclic control and the roll rate is fed back to the lateral cyclic control. Control feedbacks on the stabilizer bar are modeled [2], [8] as ;

$$\frac{B_{1s}}{q} = \frac{K_B}{\tau_B s + 1} / sec \tag{2.31a}$$

$$\frac{A_{1s}}{p} = \frac{-K_B}{\tau_B s + 1} / sec \tag{2.31b}$$

where B_{1s} is the longitudinal cyclic control, A_{1s} is the lateral cyclic control, p is the roll rate, q is the pitch rate, K_B is the stabilizer bar mechanical mixing ratio gain and τ_B is the mechanical damping constant. Specific values of the constants for UH-1H helicopter are obtained from references [2] and [8]. Equations 2.31a and 2.31b shows that stabilizer bar is most effective while during maneuvers with considerably high body angular rates.

2.3 Tail Rotor Modeling

Tail rotor calculations of minimum complexity simulation model[1] consist of the same iterative method of main rotor for thrust and induced velocity but without including flapping dynamics. Although the convergence of the iteration is fast, some maneuvers especially with high yaw rates causes tail rotor iteration not to converge to normalized values. Therefore, a more robust iterative method is developed. Figure 2.7 is the schema of the developed tail rotor algorithm.

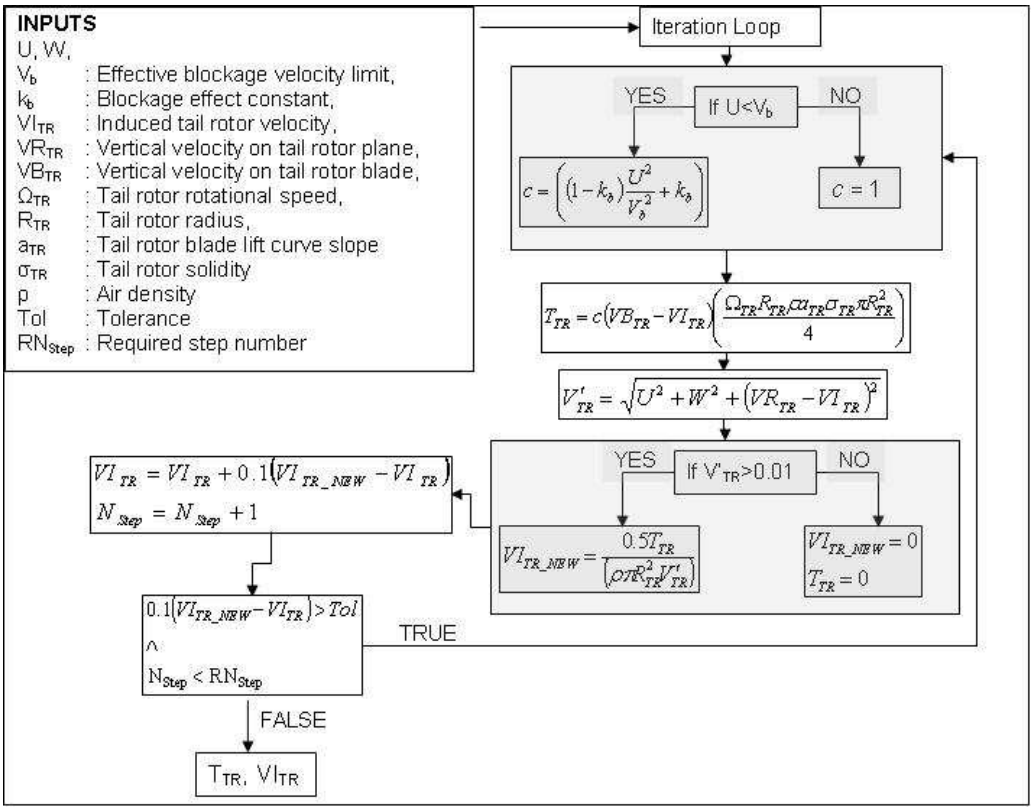

Figure 2.7: Tail rotor iteration schema

Control mapping between the pilot pedal control and root pitch angles of tail rotor blades is established by using the references [2] and [8].

In the updated tail rotor iterative calculation, blockage effect of the vertical tail is considered. Moreover, convergence of the iteration is supported by feeding back by the internal iterative errors and determining iteration steps.

2.4 Horizontal Tail Modeling

UH-1H helicopter has a stabilizer type horizontal tail, which changes the incidence angle by changing pilot longitudinal cyclic. According to data in reference [2], the mechanical linkage is modeled. Data is fitted to a curve and an analytical expression for the mechanical connection is obtained as a 3^{rd} order polynomial form. The curve fitted data is shown in figure 2.8.

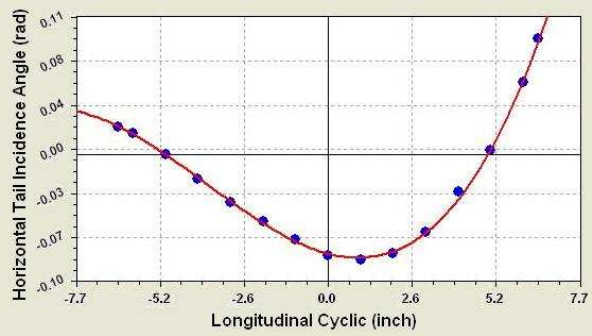

Figure 2.8: Longitudinal cyclic vs horizontal tail incidence angle

Originally, the minimum complexity simulation model [1] uses a quadratic lift form for the calculations of the horizontal stabilizer. According to this approach, the stall of the horizontal tail is checked and if stalled, a new set of constants are used for the calculations. This transition leads to a discontinuity throughout the calculations and especially was causing numerical instabilities in the trim solution. Hence, in the updated model a new simplified aerodynamics based approach is used. Firstly, the angle of attack of the horizontal tail is calculated considering the real-time incidence change through pilot longitudinal input and real-time main rotor inflow effects on the platform. Also, airfoil test data of the horizontal tail are obtained from

literature [14] for 180 degrees of angle of attack. For Reynold's number changing from 80000 to 10000000, each data is fitted to curves which are composed of 6^{th}, 7^{th} or/and 8^{th} degree polynomials. Since the horizontal tail is a simple rectangular platform with symmetrical airfoil shape, three dimensional effects are ignored and empirical airfoil sectional properties are applied to whole horizontal tail platform. Note that at some portions of the graphs, the angle of attack as hşgh as 180 degrees, which is an indication of reverse flow. Some curve fitted data is shown in figures 2.9 and 2.10 ;

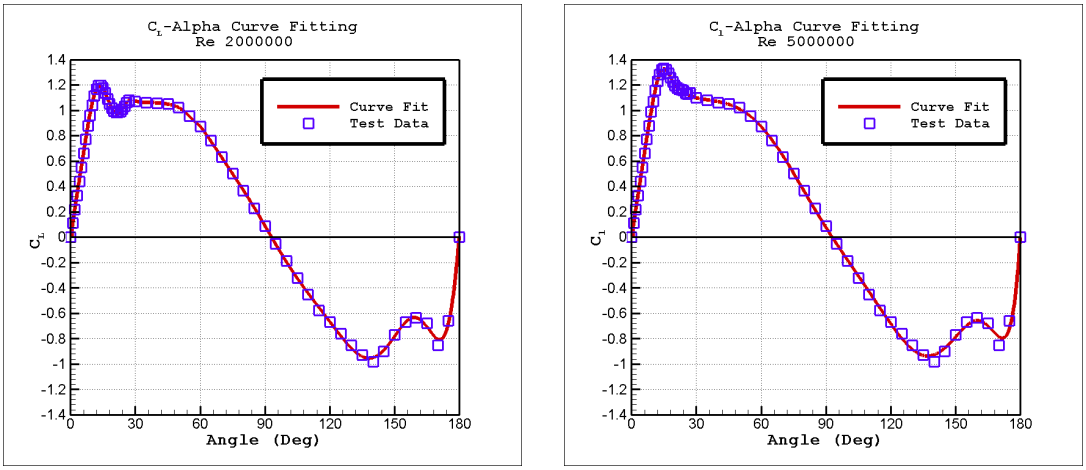

Figure 2.9: C_l vs angle of attack curves fitted to test data for various Reynold's numbers

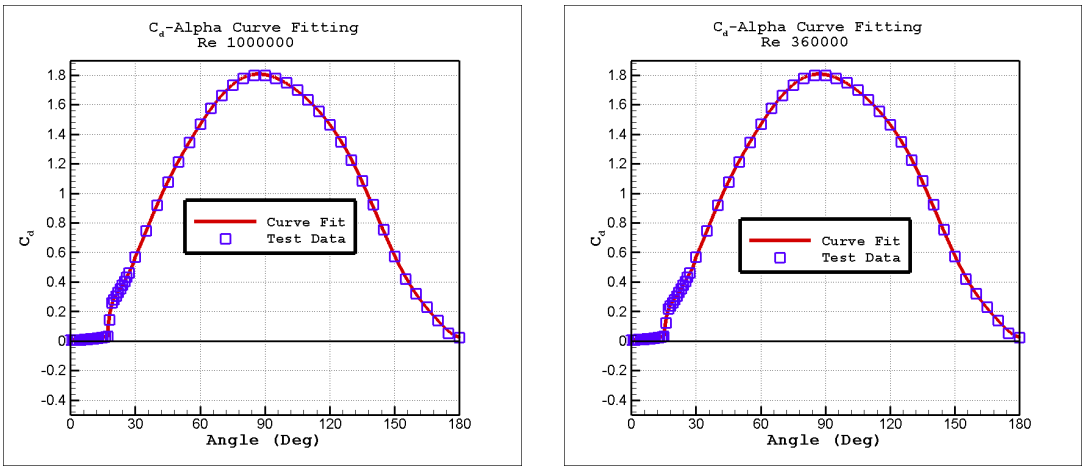

Figure 2.10: C_d vs angle of attack curves fitted to test data for various Reynold's numbers

Next, Reynold's number (Re) of the airfoil for the instantaneous flight condition is calculated as [15] :

$$Re = \frac{\rho V_{Local} c_{mean}}{\mu_d} \tag{2.32}$$

where

$$\mu_d = 373.(10)^{-9}(\frac{T_R}{519})^{1.5}\frac{717}{T_R + 198} \tag{2.33}$$

ρ is the density of the air ($slug/(ft)^3$), V_{Local} is the local velocity of the air (ft/sec), c_{mean} is the mean aerodynamic chord of the horizontal tail (ft), μ_d is the dynamic viscosity of the air (Pound force seconds/ft^2) and T_R is the temperature of the air (Rankine). After calculating the Reynold's number, the interval is determined to which the instantaneous value belongs to. Then, the corresponding C_L and $C_{d,0}$ values are determined. Then, knowing the angle of attack, a linear interpolation using the calculated Reynold's number is used to calculate the C_L and $C_{d,0}$ values. Since the test data is collected for Reynold's numbers between 80000 and 10000000, lower and higher values are bounded to these limit values. Drag coefficient of the horizontal tail is calculated by equation 2.34 :

$$C_D = C_{d,0} + \frac{C_L^2}{\pi A R e} \tag{2.34}$$

where $C_{d,0}$ is the drag coefficient of the horizontal tail airfoil, C_L is the coefficient of the lift, "AR" is the aspect ratio and "e" is the span efficiency. Span efficiency of the horizontal tail is assumed as 0.9.

Finally, real time total drag and lift forces on the horizontal tail are calculated. Therefore, stall cases are included through coefficients of lift and drag for all angle of attack values. Moreover, analytic form resulted in continuous calculations throughout the iterations. During this approach, effects of compressibility and Mach number is neglected. Instead of non-uniform induced flow interaction, the horizontal tail is assumed to be effected by averaged normal component of the induced velocity. Also, swirl effects of inflow and highly turbulent interactions of tail boom, main and tail rotors on horizontal tail are neglected. Some advanced methods and detailed experiments about interactions can be found in references [16], [17] and [18].

2.5 Vertical Tail Modeling

Both the updated and the minimum complexity simulation models simulate the vertical tail with the quadratic form expressions. There is a lack of information about vertical tail airfoil section, sweep back angle, taper ratio and thickness variation. Moreover, vertical tail is very close to the tail rotor inflow region. Therefore, modeling the vertical tail with simplified aerodynamics similar to the horizontal tail, is thought to be as a future work. Unlike the minimum complexity model, incidence of the vertical tail is included in the updated model calculations.

2.6 Fuselage Modeling

Minimum complexity model uses quadratic form expressions for the fuselage. On the other hand, the updated model includes aerodynamic derivatives of the UH-1H fuselage [8], [2]. Main rotor induced velocities effect are included both in the minimum complexity and the updated model.

2.7 Skid Modeling

Forces and moments on skids are calculated by modeling the skids as four imaginary landing gears composed of spring-damper systems, which are located at corners of skids. Geometrical positions of the landing gears w.r.t. center of gravity of the helicopter are listed in table 2.1. It is assumed that front and rear landing gears are symmetrical about to the center of gravity. Since four independent spring-damper type landing gears are modeled, different landing scenarios are available with various landing gear touch down conditions.

Table 2.1: Position of the imaginary landing gears w.r.t the center of gravity of the body axis

	x_{gear}(ft)	y_{gear}(ft)	z_{gear}(ft)
Left Front Landing Gear	7.25	-3.75	4.79
Right Front Landing Gear	7.25	3.75	4.79
Left Aft Landing Gear	-7.25	-3.75	4.79
Right Aft Landing Gear	-7.25	3.75	4.79

Velocity vector of the landing gears in the body frame are found from;

$$\vec{V}_{gear} = \vec{V}_{helicopter} + \vec{\omega} \times \vec{r}_{gear} \tag{2.35}$$

where $\vec{r}_{gear}$ is the position vector of the gears w.r.t the center of gravity in the body axis , $\vec{\omega}$ is the body angular rates and $\vec{V}_{helicopter}$ is the velocity vector of the helicopter in body axis.
For each landing gear ;

$$\vec{V}_{helicopter} = u_{body}\vec{i} + v_{body}\vec{j} + w_{body}\vec{k} \tag{2.36}$$

$$\vec{\omega} = p\vec{i} + q\vec{j} + r\vec{k} \tag{2.37}$$

$$\vec{r}_{gear} = x_{gear}\vec{i} + y_{gear}\vec{j} + z_{gear}\vec{k} \tag{2.38}$$

Finally, after substituting equations 2.36,2.37 and 2.38 into the 2.35 , resulting velocities of each landing gear are :

$$u_{gear} = u_{body} + qz_{gear} - ry_{gear} \tag{2.39}$$

$$v_{gear} = v_{body} - pz_{gear} + ry_{gear} \tag{2.40}$$

$$w_{gear} = q_{body} + py_{gear} - qx_{gear} \tag{2.41}$$

where p, q, r are the roll, pitch and yaw angular rates respectively.

For the landing phase of the real time simulation flight scenarios, a structural crash of the skids after a harsh landing is not included in the model. On the contrary, since skids are able to function even with a very high decent velocity, they create instantaneously high forces and moments in the center of gravity of the helicopter when helicopter touches the ground. Due to the sudden high force and moments, mathematical model tends to diverge. This leads to crash mode and visual system freezes after the crash. Therefore, pilot understands that skids are broken due to harsh landing.

2.8 Ground Surface Reaction Modeling

The sequence of calculation of ground reactions is as follows:

- Firstly, force on the landing gear is calculated by equation 2.42 when it touches the ground surface.

$$F_{gear} = -c\dot{x}_c - kx_c \tag{2.42}$$

where c is the damping coefficient and k is the spring coefficient of the landing gears, x_c is the compression length and $\dot{x}_c$ is the compression rate of the landing gears. At the beginning, c and k were approximated according to existing values for helicopter model in Ref [11]. Then fine tuning was performed while testing in simulation environment. For each landing gear, height above the ground is calculated and compression length is checked for compressed case, which means the touch down condition. If the landing gear is compressed, then the force acting on it is calculated by equation 2.42.

- For each landing gear, after obtaining the force on the landing gear, normal force (N) is calculated as :

$$N = \frac{F_{gear}}{\cos\theta \cos\phi} \tag{2.43}$$

where θ and ϕ are pitch and roll Euler angles respectively.

- For the calculations of frictional forces on ground, the coefficients of static and dynamic friction forces are obtained from Ref [4]. Although the mathematical model is able to land different types of ground surfaces (grass, airport, soil, various helipads, etc.) throughout the simulation environment, it is assumed that the friction properties of the ground remain same for all landing cases. Equation 2.44 is used for calculating resultant friction coefficient with the experimental values of the UH-1H skid properties [4].

$$\mu_c = f_d + (f_s - f_d)e^{-\beta_f |V_{rel}|} \tag{2.44}$$

where f_d is the dynamic coefficient of friction, f_s is the static coefficient of friction, β_f is the exponential coefficient of decay and V_{rel} is the relative velocity of the surface on contact. Same friction properties are used for forward and side ward friction cases of the skid.

- After obtaining the skid friction values, friction forces on the ground in both forward (F_{fx}) and side ward (F_{fy}) directions are calculated by using the normal forces.

$$F_{fx} = \mu_c |N| signum(u_{gear}) \tag{2.45}$$

$$F_{fy} = \mu_c |N| signum(y_{gear}) \tag{2.46}$$

- Finally, frictional forces of each landing gear are carried to the center of gravity of the helicopter. To include the friction forces in the equations of motions of the helicopter, they are transformed according to the pitch and roll Euler angles,θ and ϕ respectively. The transformed forces (F_{lgX},F_{lgY},F_{lgZ}) are obtained by the following equation.

$$\begin{Bmatrix} F_{lgX} \\ F_{lgY} \\ F_{lgZ} \end{Bmatrix} = \begin{bmatrix} \cos\theta & 0 & -\sin\theta \\ \sin\theta\sin\phi & \cos\phi & \cos\theta\sin\phi \\ \sin\theta\cos\phi & -\sin\phi & \cos\theta\cos\phi \end{bmatrix} \begin{Bmatrix} F_{fx} \\ F_{fy} \\ N \end{Bmatrix}$$

  Therefore, any ground reaction on any landing gear is included on the whole dynamics of the simulated helicopter instantaneously.

2.9 Altitude and thrust coefficient updating

Minimum complexity simulation model[1] uses the sea level assumption for the full flight envelope calculations. However, UH-1H is a utility helicopter and possible flight envelopes may contain high altitude missions. In the updated model, effects of altitude on air density and performance of the helicopter are included. Following formulations are used to calculate the temperature and air density for the given altitude.

Temperature at any altitude is:

$$T_{ISA} = T_{SL} - 6.5h * 0.0003048009 \tag{2.47}$$

where T_{ISA} is the temperature at the given altitude is in standard atmospheric conditions in Kelvin, T_{SL} is the standard sea level temperature in Kelvin and h is the given altitude in feet.

Density at any altitude is:

$$\rho = \rho_{SL}\left(\frac{T_{ISA}}{T_{SL}}\right)^{4.256} \tag{2.48}$$

where ρ is the density of the air at given altitude in slug/$feet^3$, ρ_{SL} is the density of air at sea level in standard atmospheric conditions in slug/$feet^3$.

Minimum complexity simulation model[1] calculates the coefficient of thrust by assuming that thrust equals to weight and it uses same thrust coefficient throughout the whole flight

envelope. On the contrary, during the real flight, thrust values and orientations generally change considerably for various conditions by pilot inputs and tip path plane orientation. Therefore, in the updated model, instantaneous thrust and air density are used for calculation of the thrust coefficient.

2.10 Ground Effect Modeling

For the treatment of ground effect, an approximate formula based on Cheseeman and Bennett's analysis is used. This thrust relationship can be expressed by the following equation [39]:

$$\left[\frac{T_{IGE}}{T_{OGE}}\right] = \frac{1}{1 - \frac{1}{16}(\frac{R}{Z})^2 \frac{1}{1+(\frac{V_f}{V_i})^2}} \tag{2.49}$$

where R is the rotor radius, Z is the height of the rotor hub above the ground, V_f is the forward velocity and V_i is the average induced velocity at the rotor.

This formula shows a good agreement with the flight test measurements of various helicopters at hover condition as shown in the figure 2.11.

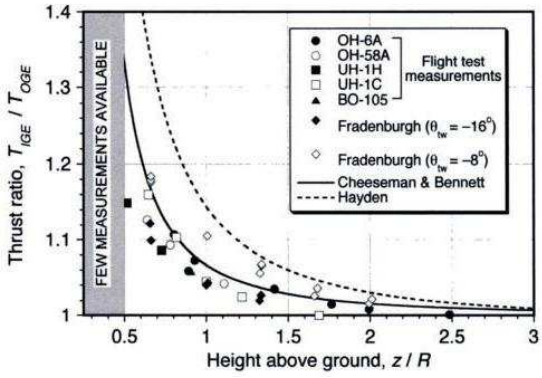

Figure 2.11: Thrust ratio versus hub altitude to main rotor radius ratio at hover for a variety of helicopters[5]

It is concluded that the results obtained from equation2.49 are not close enough to the flight test measurements for UH-1H. While considering measurements of UH-1H, a significant reduction in thrust ratio is observed near the ground. Hence, equation 2.49 is modified based on the data in the figure 2.11.

$$\left[\frac{T_{IGE}}{T_{OGE}}\right] = \frac{1}{1 - K\frac{1}{16}(\frac{R}{Z})^2 \frac{1}{1+(\frac{V_f}{V_i})^2}} \tag{2.50}$$

For modification, K is selected as 0.62 by adjusting the equation 2.49 to flight test data for UH-1H [5]. The difference can be seen in the figure 2.12

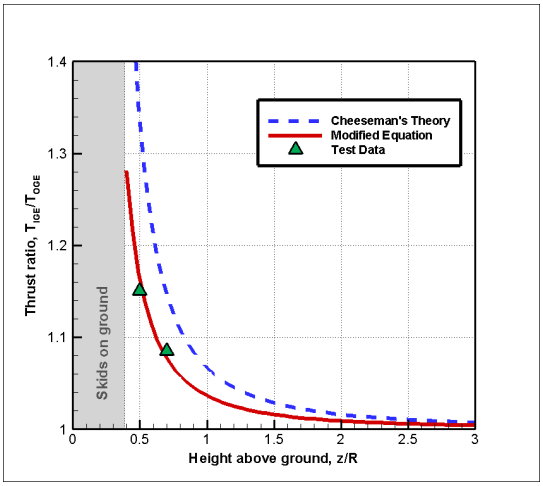

Figure 2.12: The modification of the Cheeseman's equation for fitting UH-1H measurement data.

After modifying the equation 2.49, the thrust versus z/R ,hub altitude to main rotor radius ratio, graphs are plotted for the hover and 30 knots forward flight conditions. With increasing velocity, thrust ratio decreases as shown in figure 2.13 which agrees with the statement in reference [5].

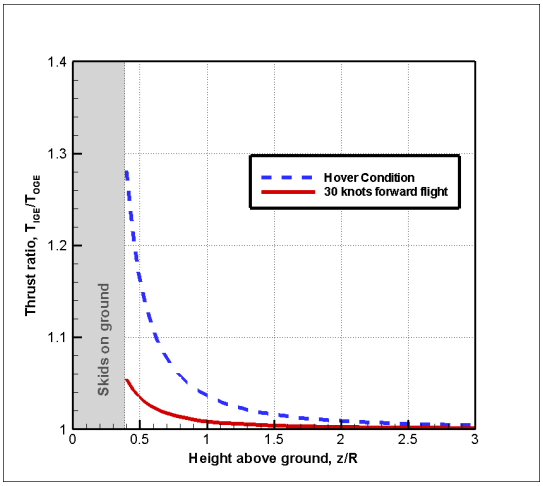

Figure 2.13: Thrust ratio versus hub altitude to main rotor radius ratio at hover condition and 30 knots forward flight condition

2.11 Other Updates

The translational motion of the helicopter in the body-fixed coordinate system is modeled in the minimum complexity simulation model [1] as reduced forms of the actual theoretical equations. Although this approach is reasonable for steady flight, effects of the maneuvers with high angular rates produce significant errors. Therefore, in the updated model all the reduced terms are restored in the equations of motion to include the effects of transient dynamics during maneuvers. The following equation set is used for the calculations of angular accelerations of body at the center of gravity of the helicopter. The marked terms do not exist in the minimum complexity model, whereas updated model includes all the present terms including the marked ones.

$$\dot{p} = [L + \overbrace{qr(I_Y - I_Z)}]\frac{\overbrace{I_Z}}{I_X \underbrace{I_Z - I_{XZ}I_{XZ}}} + \overbrace{[N + pq(I_X - I_Y)]\frac{I_{XZ}}{I_X.I_Z - I_{XZ}I_{XZ}}} \tag{2.51a}$$

$$\dot{q} = \frac{M}{I_Y} - pr\frac{(I_X - I_Z)}{I_Y} \tag{2.51b}$$

$$\dot{r} = [L + \underbrace{qr(I_Y - I_Z)}\frac{I_{XZ}}{I_X I_Z - \underbrace{I_{XZ}I_{XZ}}} + [N + \overbrace{pq(I_X - I_Y)}]\frac{\overbrace{I_X}}{I_Z \underbrace{I_X - I_{XZ}I_{XZ}}} \tag{2.51c}$$

In addition, the minimum complexity simulation model [1] uses reduced order velocity transformation matrices for the conversion of the body frame to the earth fixed frame instead of the actual theoretical transformation equations. The helicopter can be subjected to high Euler angles and simplified transformations tend to cause significant errors. Hence, full transformation matrices are used in the updated model in order to be able to simulate the high Euler angle flight conditions. The restored terms, which are included in updated model, are marked in the following transformation equation.

$$\begin{Bmatrix} \dot{x_e} \\ \dot{y_e} \\ \dot{z_e} \end{Bmatrix} = \begin{Bmatrix} \cos\theta\cos\psi & \overbrace{\sin\theta\sin\phi\cos\psi - \cos\phi\sin\psi} & \sin\theta\cos\phi\cos\psi + \overbrace{\sin\phi\sin\psi} \\ \underbrace{\cos\phi}\ \sin\psi & \underbrace{\sin\theta\sin\phi\sin\psi} + \cos\theta\cos\psi & \sin\theta\cos\phi\sin\phi - \sin\phi\cos\psi \\ -\sin\theta & \underbrace{\cos\theta\sin\phi} & \cos\theta\cos\phi \end{Bmatrix} \begin{Bmatrix} U \\ V \\ W \end{Bmatrix} \tag{2.52}$$

CHAPTER 3

TRIMMING USING A FLIGHT CONTROLLER

Unlike most fixed wing aircraft, helicopters are inherently unstable vehicles especially at hover and low speed flights. Also, due to high frequency rotor dynamics and highly coupled responses, helicopters require more pilot workload when compared to fixed wing aircrafts. Therefore, trimming a helicopter is a sophisticated and arduous work for pilots. In the case of simulation models, trimming is also a challenging task as it will require a numerical solution to highly non-linear equations. [29].

There are several ways to design a trimming procedure for a helicopter simulation model. One way is to use a numerical optimization method, that would find the states, that sets all state derivatives equal to zero. In this thesis, a flight control system is used for the trimming process. The control system forces the dynamic model in time to reach a certain trim state. Then the simulation is stopped and the resulting aircraft and control states define a trim condition.

The controller used in this thesis for trim consists of two loops: An inner loop and an outer loop. In the inner loop, the rotational states are controlled in the roll, pitch and yaw channels, whereas in the outer loop east and north velocities are controlled along with the altitude. Decoupling of the inner and outer loop is possible since the dynamics of the rotational states are much faster than the dynamics of translational states. Therefore, the rotational states are controlled in the inner loop and the translational states in the outer loop. The block diagram of the control system developed is shown in figure 3.1.

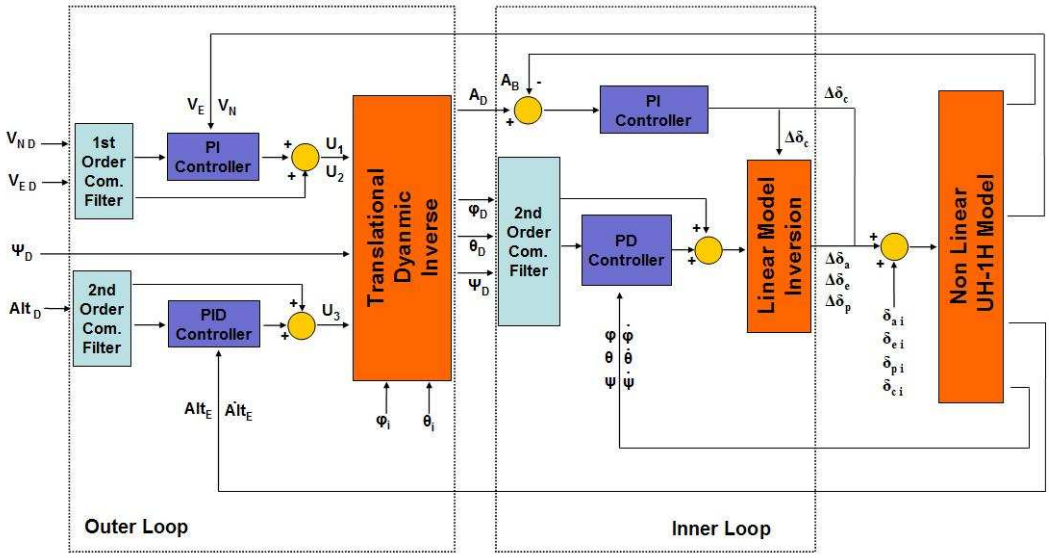

Figure 3.1: Block Diagram of the Control System

3.1 Inner Loop Controller

The rotational states are controlled in the inner most loop of the controller. Euler angles, ϕ, θ, and ψ, are commanded to the inner loop along with the total linear acceleration command and it generates longitudinal cyclic, lateral cyclic, pedal and collective control deflections to the mathematical model. This loop is often called the stabilization loop. The total linear acceleration command generated by the outer loop is used with the linear acceleration feedback from the aircraft to generate the collective control deflection. A PI controller is used for this process [20] (figure 3.1) . Pitch and roll commands are generated in the outer loop, whereas yaw command is directly input by the user. All of the Euler angle commands are passed through a second order command filter, a low pass filter, to match the performance of the aircraft to the commands. Each of these channels are controlled using a PD controller. The second derivative of the commands, generated by the command filter, in each channel is used in a feed forward path as a command accelerator. Longitudinal cyclic, lateral cyclic and pedal controls are generated by using linear model inversion [21], [22], [23] (figure 3.1). Linear model inversion is derived from the decoupled linear state space representation. Decoupling

is done between the fast rotational states, Euler angles, and fast translational states:

$$\begin{Bmatrix} \delta_a \\ \delta_e \\ \delta_p \end{Bmatrix} = B^{-1}(\begin{Bmatrix} \dot{p_c} \\ \dot{q_c} \\ \dot{r_c} \end{Bmatrix} - A_1 \begin{Bmatrix} u \\ v \\ w \\ \delta_c \end{Bmatrix} - A_2 \begin{Bmatrix} p \\ q \\ r \end{Bmatrix}) \tag{3.1}$$

where, δ_c, δ_a, δ_e and δ_p are the deflections of the collective, lateral, longitudinal and pedal controls respectively, B is the linear control matrix, A_1 and A_2 are stability matrices, $\dot{p_c}$, $\dot{q_c}$ and $\dot{r_c}$ are desired rotational accelerations, u, v, w and p, q, r are body velocity and rotational angular rates respectively which are fed back from the mathematical model.

3.2 Outer Loop Controller

The outer loop is responsible for the generation of the roll and pitch commands [19] along with the acceleration command [20] for the inner loop. It is also called the navigation loop. The outer loop requires north and east velocity, altitude and heading commands. These commands are input by the user. Similar to the one in the inner loop, a command filter is present in the outer loop. The velocity commands are passed through a first order command filter, whereas the altitude command is passed through a second order command filter. The two velocity channels are controlled by a PI controller and the altitude channel is controlled by a PID controller. Similar to the inner loop, accelerations generated in the command filter are fed forward as command accelerators figure 3.1. Outputs of the linear controllers, U_1, U_2 and U_3 are used to generate acceleration, roll and pitch commands. The total acceleration command is calculated by the following formula:

$$A_D = \sqrt{U_1^2 + U_2^2 + (U_3 - g)^2} \tag{3.2}$$

Roll and pitch commands are generated using the transformation between the earth and body acceleration.

$$\begin{Bmatrix} \ddot{X} \\ \ddot{Y} \\ \ddot{Z} \end{Bmatrix} = L_{VB}(\phi, \theta, \psi) \begin{Bmatrix} F_x/m \\ F_y/m \\ F_z/m \end{Bmatrix} + \begin{Bmatrix} 0 \\ 0 \\ g \end{Bmatrix} \tag{3.3}$$

where, X, Y, Z are positions in north-east-down earth fixed coordinate system, L_{VB} is the orthogonal transformation matrix from body fixed to earth fixed frame, F_x, F_y, F_z are force components in the body fixed coordinate axis. In equation 3.3, accelerations in the north-east-down earth fixed coordinate system are replaced with acceleration commands U_1, U_2 and U_3:

$$\begin{Bmatrix} U_1 \\ U_2 \\ (U_3 - g) \end{Bmatrix} = L_{VB}(\phi, \theta, \psi) \begin{Bmatrix} F_x/m \\ F_y/m \\ F_z/m \end{Bmatrix} \tag{3.4}$$

Furthermore, by using equation 3.4, the desired roll and pitch angles can be calculated by the formulae in equation 3.5 and 3.6. In this derivation, it is assumed that the cyclic and pedal control forces are much smaller compared to the collective control force. Moreover, forces in x and y direction in the body fixed frame are assumed to be small compared to forces in z direction in body fixed frame [19]:

$$\phi_D \approx \sin^{-1}\left(\frac{-U_1 \sin\psi_D + U_2 \cos\psi_D}{\sqrt{U_1^2 + U_2^2 + (U_3 - g)^2}}\right) + \phi_i \tag{3.5}$$

$$\theta_D \approx \tan^{-1}\left(\frac{U_1 \cos\psi_D + U_2 \sin\psi_D}{(U_3 - g)}\right) + \theta_i \tag{3.6}$$

where ψ_D is the heading command, θ_D and ϕ_D are pitch and roll commands respectively, θ_i and ϕ_i are initial values of pitch and roll attitudes. The detailed analysis of this control system can be found in [24].

Trimmer is run for both models until finding trimmed points of any desired flight condition. Although stability and control matrices in the trimmer belong to hover condition, trimmer performs adequately for the forward flight cases too. Moreover, trimmer do not require actuator models, which are actually important for the autopilot and stability control augmentation systems (SCAS). In this thesis, the main duty of the trimmer is finding the trimmed conditions of the simulation models for the given flight condition. As an example, trimmer is used to find the trimmed conditions of the simulation models for 30 knots forward flight case, shown in figures 3.2, 3.3, 3.4 and 3.5.

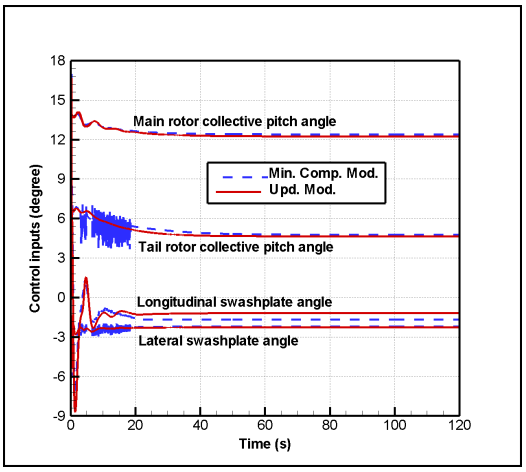

Figure 3.2: Control inputs of simulation models during trimming process.

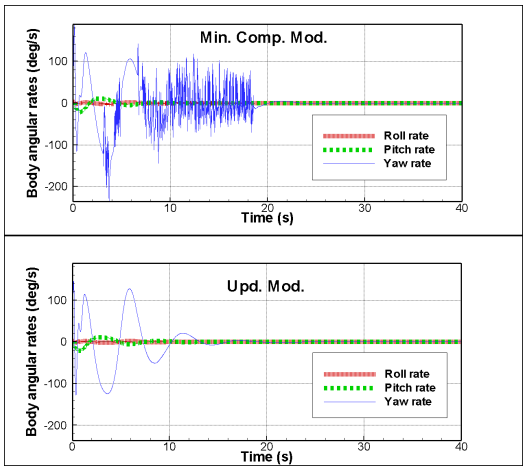

Figure 3.3: Body angular rate responses of simulation models during trimming process.

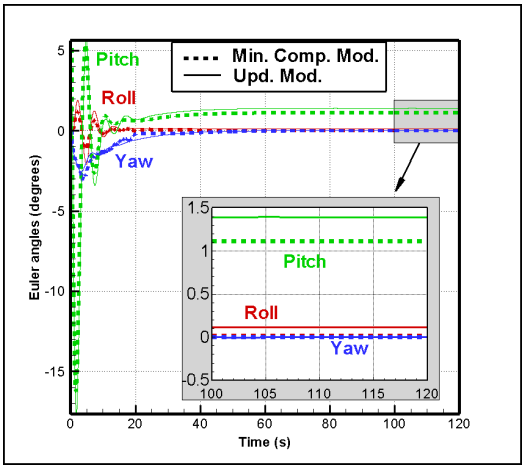

Figure 3.4: Euler angle responses of simulation models during trimming process.

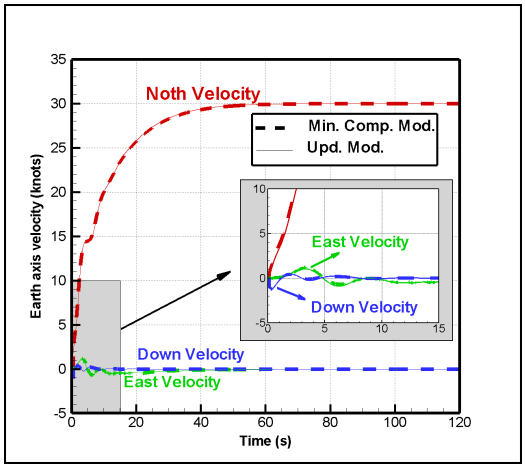

Figure 3.5: Earth velocity responses of simulation models during trimming process.

Geographical North-East-Down (NED) frame is used with flat earth assumption. Therefore, according to Euler transformation, North velocity is the forward velocity at zero yaw angle. It is observed that minimum complexity model has oscillatory characteristics during trimming process mainly due to discrete component stall and tail rotor calculations which tend to diverge for special cases. On the other hand, updated model shows a smoother trimming trend. Figures 3.2, 3.3, 3.4 and 3.5 indicate the difference between simulation models in the means of trimming. In spite of different trimming characteristics of the simulation models, trimmer is able to find trim conditions of both models for various forward flight conditions as illustrated for 30 knots case in figures 3.2, 3.3, 3.4 and 3.5.

CHAPTER 4

SIMULATION RESULTS AND MODEL VERIFICATION

Various simulations are run and the minimum complexity and updated simulation models are compared against available flight test data. The models are first trimmed for various forward flight velocities and the dynamic responses of the simulation models to pilot step inputs are compared with test results [2], [9], [10].

First the trim values are compared. During this verification, the helicopter weight is set to 7200 lbs and the altitude of the flight is 200ft. During the dynamic response verification, the weight of the helicopter is 6158lbs and the aircraft is out of ground effect. The reason for the difference in weights is due to the available flight test data conditions. During trim comparison, the trim values of the collective, tail, longitudinal and lateral swash plate angles of the simulation models are compared with existing flight test data. In the dynamic response comparison, body angular rate and Euler angle responses of the simulation models to control step inputs are compared with existing flight test data.

4.1 Trim Condition Validation

In references [9] and [10], trim values of main and tail rotor pitch, longitudinal and lateral swash plate angles are given for the UH-1H helicopter for forward velocities. The trimmer described in chapter 3 is used to find the trim conditions of the helicopter simulation models for various forward velocities. Abridgment ”Min. Comp. Mod.” and ”Upd. Mod.” refer to minimum complexity model and updated model respectively through the following plotted graphs.

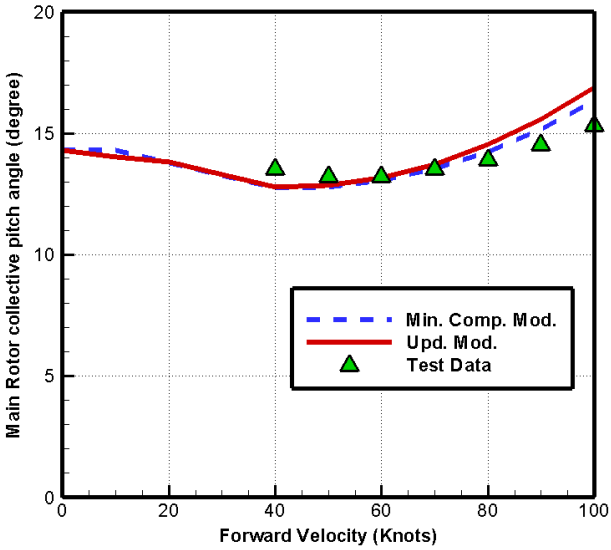

Figure 4.1: Root pitch angle of main rotor blades vs forward velocity

It is seen from figure 4.1 that both the minimum complexity and the updated model have harmonic characteristics for trim values of root pitch angles of main rotor blades for various forward velocities. Deviations from the test data is thought to be mainly because of the additional effects of main rotor inflow on horizontal stabilizer, tail boom and empennage.

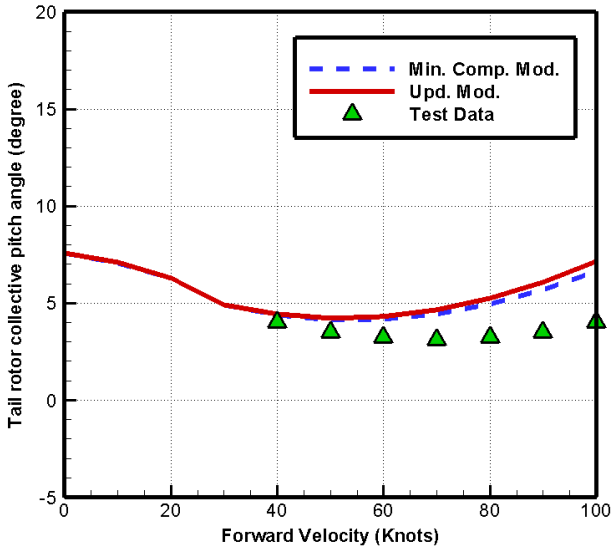

Figure 4.2: Root pitch angle of tail rotor blades vs forward velocity

Figure 4.2 shows that although both models have close root pitch angles of tail rotor blades for increasing velocities, there is a difference between the simulation model results and test data. Especially, at high velocities simulation models require higher pedal input to trim the simulated helicopter than the actual one. The reason for mismatch between simulation models and test data could be the interaction effects of the main rotor wake on the tail rotor. It must be noted that the influence of the main rotor generated wake on the helicopter tail rotor calculations is not taken into account for both simulation models.

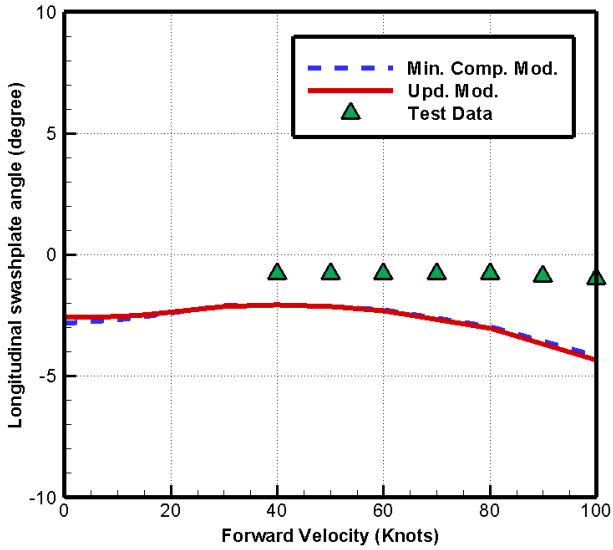

Figure 4.3: Longitudinal swash plate angle vs forward velocity

Figure 4.3 shows that both models have close longitudinal swash plate angles for trimmed flight of the simulated helicopter for increasing velocities. But there is an off-set between the simulation results and the test data. Most of the control transformations from the pilot to the swash plate mechanism is obtained from reference [8]. In reference [2], a mechanical lateral pilot cyclic rigging, which is excluded in the simulation models, is introduced as two degrees. Therefore, including the mechanical rigging is thought to shift the trim values of the longitudinal swash plate to adjacent to the test data. Moreover, including the main rotor wake effects on tail rotor calculations will probably result in a different tail rotor collective angle, thus a tail rotor thrust, which also causes a different orientation of the tip path plane mainly in the lateral direction to trim the helicopter simulation model. This will require a new lateral pilot cyclic leading to different longitudinal swash plate angle.

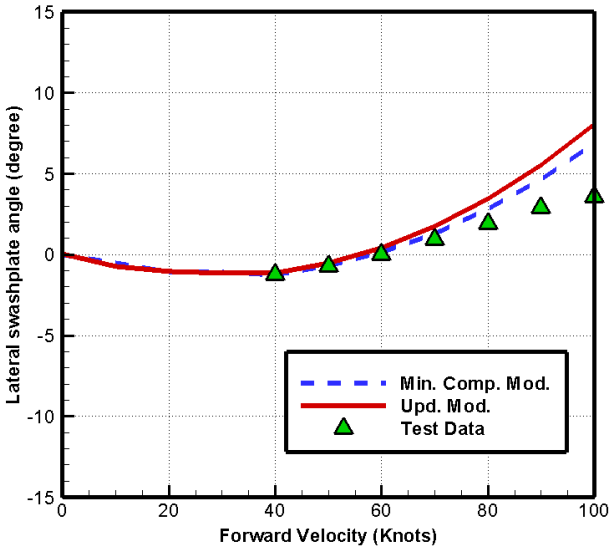

Figure 4.4: Lateral swash plate angle vs forward velocity

It is observed from figure 4.4 that both simulation models have close results for lateral swash plate angles of trimmed conditions for increasing velocities. Especially for high velocities, models require higher lateral swash plate angles to trim the simulation models than lateral swash plate angles of the real helicopter. Considering the difference between the simulation results and test data, including advanced influences of main rotor wake like swirl effect implemented wake models on horizontal tail will change the trimmed conditions of the longitudinal cyclic which is connected to the horizontal stabilizer nonlinearly.

Graphics of trimmed flight conditions for various forward velocities showed that both simulation models have close swash plate, main and tail rotor blade root pitch angles. Although there are deviations from the test data, trimmed control angles of both models capture the general trends of test data for the increasing forward velocities.

4.2 Dynamic Response Validation

For the investigation of the dynamic responses of the simulation helicopter models in the time domain, step inputs are applied to the pilot controls after one second of trimmed flight. Reference [2] reports two different flight tests for hover and 60 knots forward flight condition.

Both minimum complexity and updated models are trimmed for hover and 60 knots. Results of the dynamic responses of the simulation models to the applied pilot step controls, which are applied to the trimmed simulation models are compared with the test data.

It is worth to mention that, since trimming a real helicopter is a hard task for the pilots and calibration conditions of embedded flight measurement devices are unknown, the test data is not perfect. For example in trim body angular rates are not exactly equal to zero. Moreover, the measured Euler angles in trim are different for the same flight conditions. In addition, wind information on the day of flight testing is also unavailable, which may have a significant effect on the helicopter responses. Similarly, no variation in weight and center of gravity of the helicopter was recorded. As a result, although the flight test is not perfect, it will still give a good idea about the dynamic response of the aircraft.

4.2.1 Hover Condition

After trimming both the minimum complexity and the updated simulation models in hover condition, a step input of one inch is applied to each pilot input axis. The time domain responses of the models are compared with the existing flight test data.

4.2.1.1 Pilot Collective Step Input

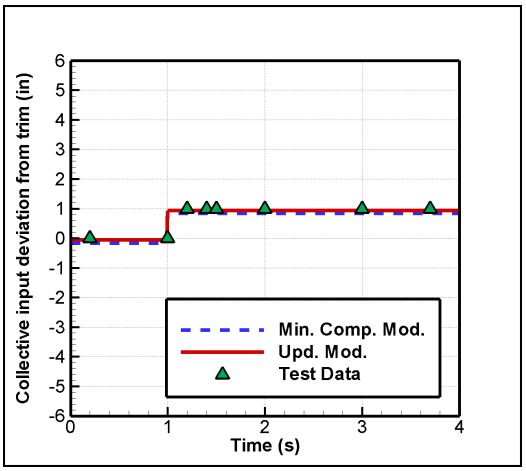

Figure 4.5: A step input of one inch pilot collective after one second of trimmed flight.

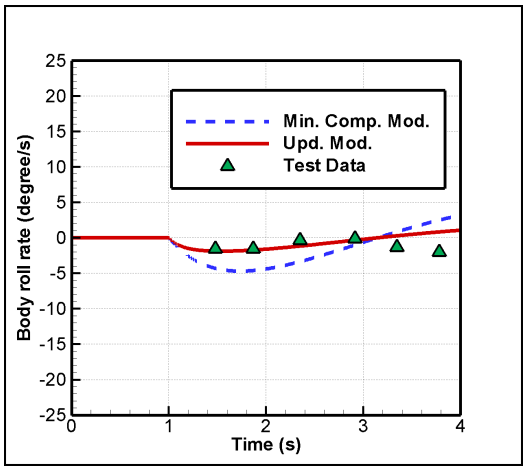

Figure 4.6: Roll rate response of the simulation models and test data.

Figure 4.5 shows the deviation of applied pilot step input on the collective control. The most dominant effect of the increasing pilot collective lever is the sudden increase in thrust and torque of the main rotor and without any other control deviation, the primary response is expected to be seen in the body yaw rate due to the increase in main rotor torque. Thus, helicopter tends to change the yaw direction while climbing. However, coupled responses appear after few seconds depending on the helicopter configuration and condition. The body roll rate response of the helicopter models and flight test data are shown in figure 4.6. It is seen that the minimum complexity model has a higher rate response than the updated model. Moreover, a more undamped response is observed for the minimum complexity model, while updated model has a close response characteristics to the flight test data.

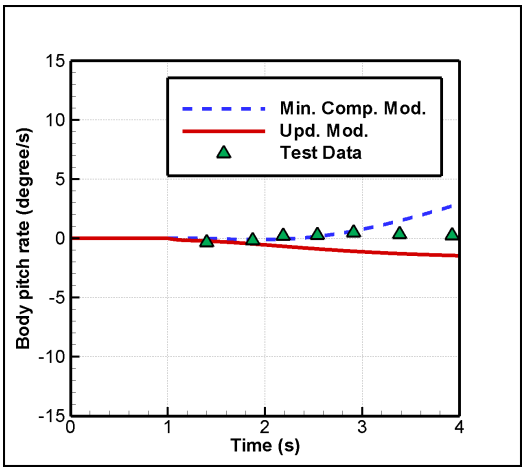

Figure 4.7: Pitch rate response of the simulation models and test data.

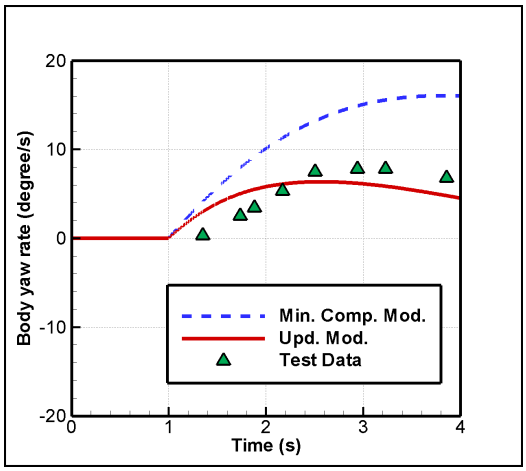

Figure 4.8: Yaw rate response of the simulation models and test data.

Figures 4.7 and 4.8 show the body pitch and yaw rate responses respectively, resulting from a step collective input. Body pitch rate response of the minimum complexity model tends to diverge from flight test data. On the other hand, the updated model has a better response even though the exact values are slightly different from the test data. As for the primary response, the minimum complexity model has a highly over predicted yaw rate response, almost twice the flight test data. The updated model accomplished a similar response to the flight test data. Figure 4.8 remarks the difference between the models and flight test data. Even tough both models stabilized the yaw rate responses after almost two seconds of disturbed flight, updated model resulted in a closer yaw rate of flight test data.

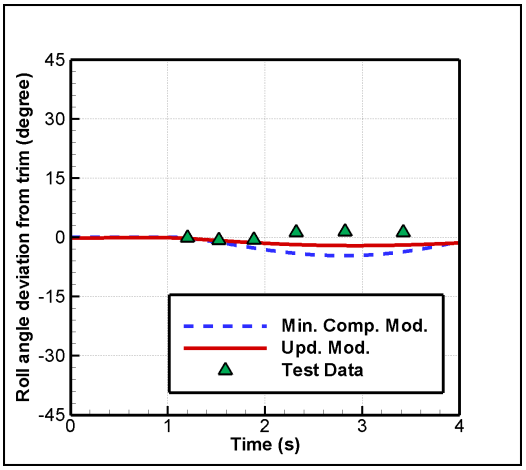

Figure 4.9: Euler roll angle response of the simulation models and test data.

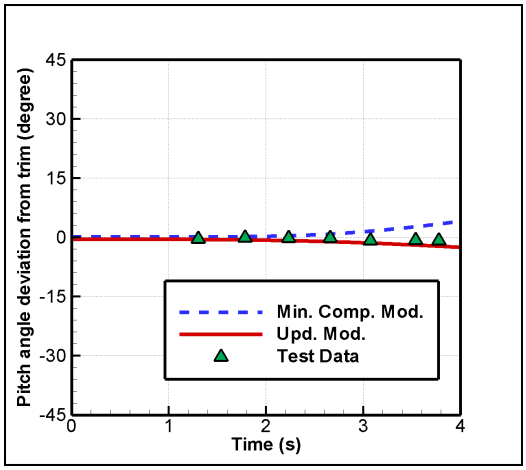

Figure 4.10: Euler pitch angle response of the simulation models and test data.

As seen from figure 4.9, updated model is closer to flight test data, with mainly constant roll angles. A similar response is observed in the Euler pitch angles in figure 4.10. Both models slightly deviate from the initial values but updated model matches test data better than the minimum complexity model.

4.2.1.2 Pilot Longitudinal Cyclic Step Input

One inch step input is applied to the pilot longitudinal cyclic after one second of trimmed flight, shown in figure 4.11. Due to the applied step longitudinal cyclic input, both models coincide with flight test data as shown in figure 4.12.

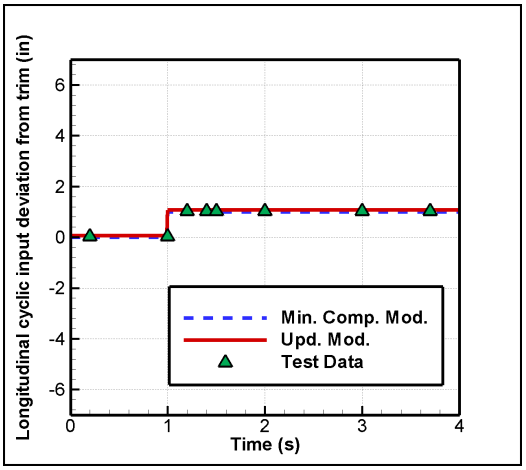

Figure 4.11: A step input of one inch pilot longitudinal cyclic after one second of trimmed flight.

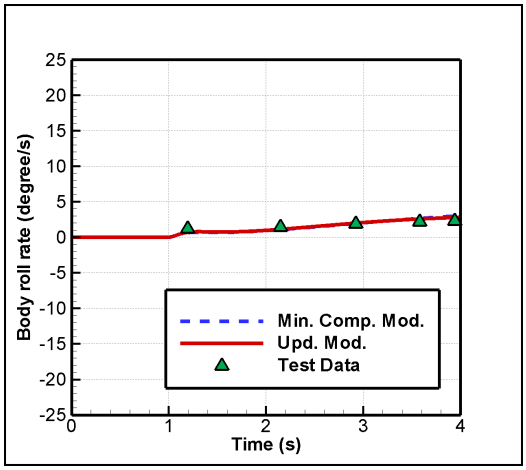

Figure 4.12: Roll rate response of the simulation models and test data.

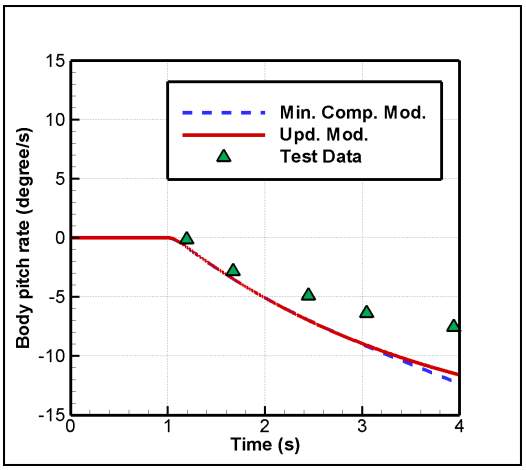

Figure 4.13: Pitch rate response of the simulation models and test data.

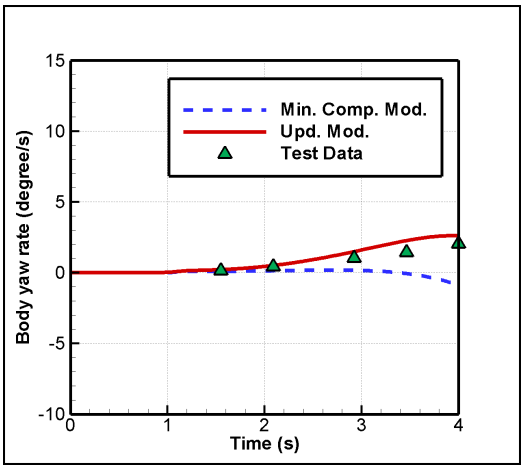

Figure 4.14: Yaw rate response of the simulation models and test data.

Figure 4.13 shows the pitch rate responses of the models and the test data to the applied step input. The figure also supports the fact that the primary response of the helicopter to a longitudinal cyclic appears in the pitch channel. Both models have the high rate responses in pitch channel when compared the other responses in roll and yaw channel. Although both models have similar rate responses, they also over predict the pitch rate response of the real helicopter according to test data. As for the yaw rate responses, updated model resulted in a better adjacency to flight test data, shown in figure 4.14.

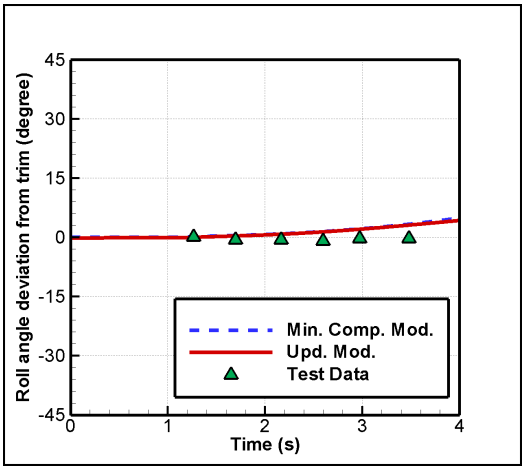

Figure 4.15: Euler roll angle response of the simulation models and test data.

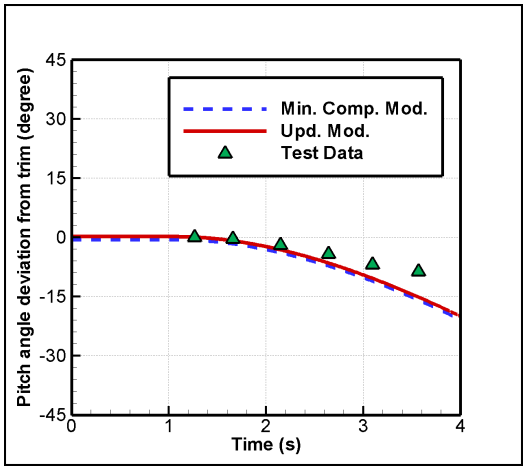

Figure 4.16: Euler pitch angle response of the simulation models and test data.

Roll angle deviations of both simulation models and test data are plotted in figure 4.15. As the dominant channel due to longitudinal cyclic input, pitch angle is the most effected Euler angle just after the control disturbance and its deviation is plotted in figure 4.16. Both models capture the pitch angle deviation of test data in a slightly over predicted manner.

4.2.1.3 Pilot Lateral Cyclic Step Input

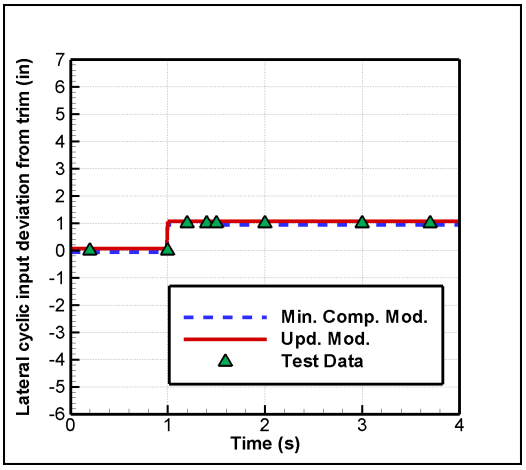

Figure 4.17: A step input of one inch pilot lateral cyclic after one second of trimmed flight.

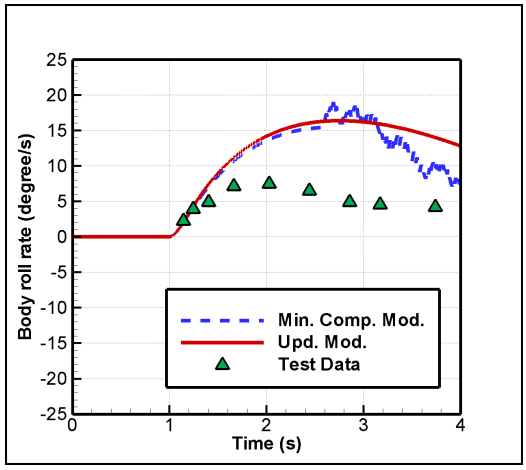

Figure 4.18: Roll rate response of the simulation models and test data.

Figure 4.17 shows the pilot lateral cyclic input, applied to a trimmed flight condition. The primary response of a lateral cyclic is seen in the roll channel (Figure 4.18). As mentioned in previous chapter, the numerical iteration of the tail rotor of the minimum complexity simulation model diverges in some cases. Figure 4.18 shows such a response. On the other hand, improved tail rotor iteration is much more reliable. It is seen that, around hover both models have higher sensitivity to the lateral cyclic when compared to the flight test data. This seems to be the biggest discrepancy of the models. The reason might be because of the lack of interaction of the inflow distribution on the fuselage and the low fidelity of the tail rotor model. These components might have induce higher damping on the lateral channel in low speeds. On the contrary, it will be shown in the 60 knots forward flight case that the roll rate response of the models mainly coincide with the test data.

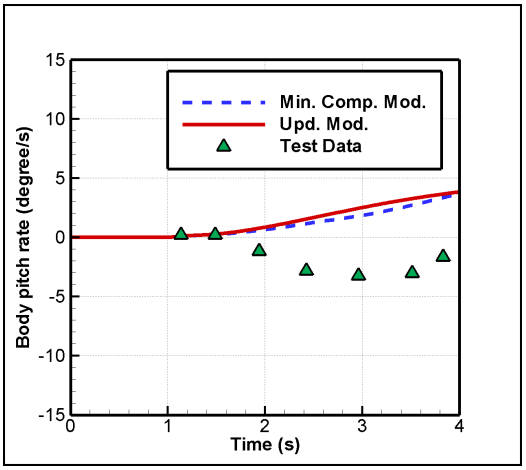

Figure 4.19: Pitch rate response of the simulation models and test data.

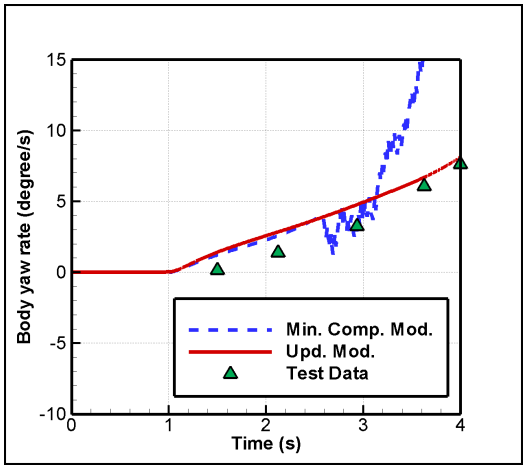

Figure 4.20: Yaw rate response of the simulation models and test data.

In the pitch rate response of the models distorted off-axis responses are observed. Off axis response is the response of the helicopter in one axis when an input was given in another axis. This distortion is mainly due to the lack of a proper modeling of the dynamic wake distortion. This well known modeling problem is dealt with in reference [60]. There, the main cause of this discrepancy is handled by including the dynamic effects of the wake. Since both models do not include off axis modifications, a reverse pitch rate response is seen in figure 4.19. Yaw rate response of the updated model is close to the flight test data, whereas the noisy outcome

of the minimum complexity exists in the yaw rate response (Figure 4.20). Same as the roll rate response, this noisy characteristics mainly belong to diverged tail rotor calculations.

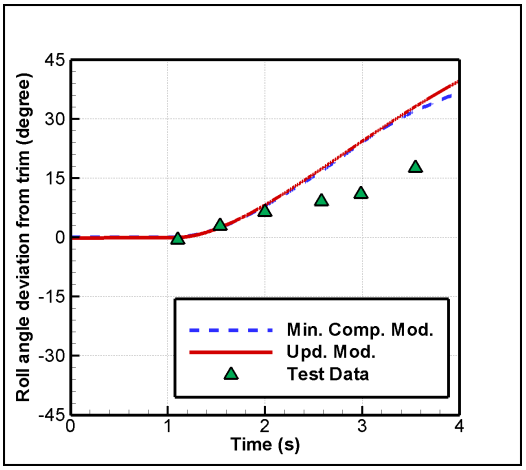

Figure 4.21: Euler roll angle response of the simulation models and test data.

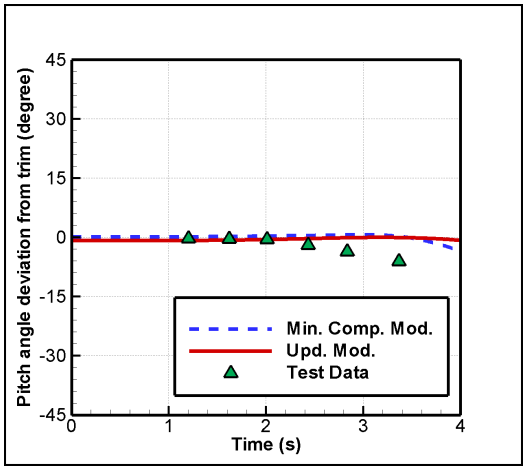

Figure 4.22: Euler pitch angle response of the simulation models and test data.

Figure 4.21 and 4.22 show the roll and pitch angles responses of the simulation models with respect to the test data, respectively. Both models kept the same pitch angle with an offset.

4.2.1.4 Pilot Pedal Step Input to Hover

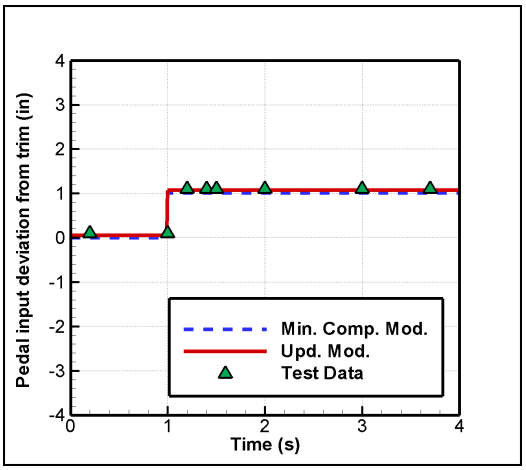

Figure 4.23: A step input of one inch pilot pedal after one second of trimmed flight.

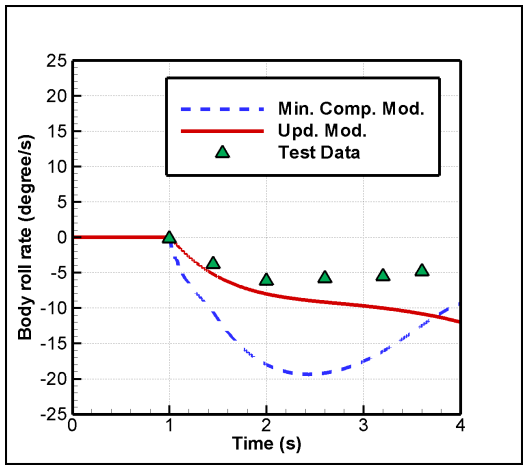

Figure 4.24: Roll rate response of the simulation models and test data.

Both simulation models and flight test data are subjected to same pilot pedal input for the trimmed hover flight as seen in figure 4.23. Minimum complexity model over predicts the roll rate response, while updated model results in a better coincidence with the flight test data as seen in figure 4.24.

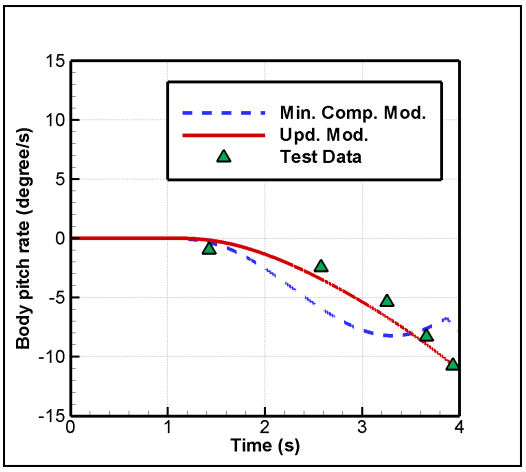

Figure 4.25: Pitch rate response of the simulation models and test data.

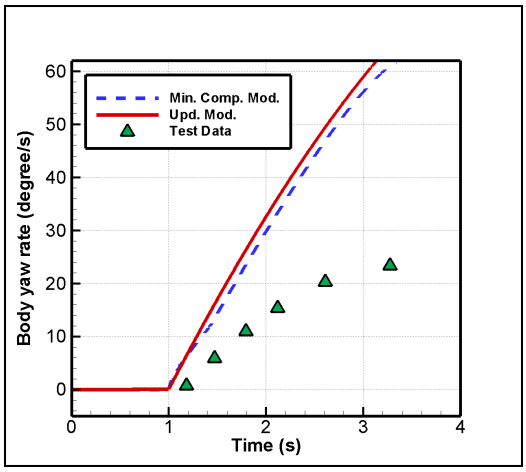

Figure 4.26: Yaw rate response of the simulation models and test data.

Pitch rate response of the updated model is well matched to the flight test data, on the contrary the minimum complexity model response shows a more divergent behavior (Figure 4.25). Both the minimum complexity and the updated models over predict the yaw rate response, which is the primary response to pilot pedal input (figure 4.26). The yaw damping of the fuselage, which is highly effected by the main rotor inflow distribution, might be included in future models for better matching to flight test data.

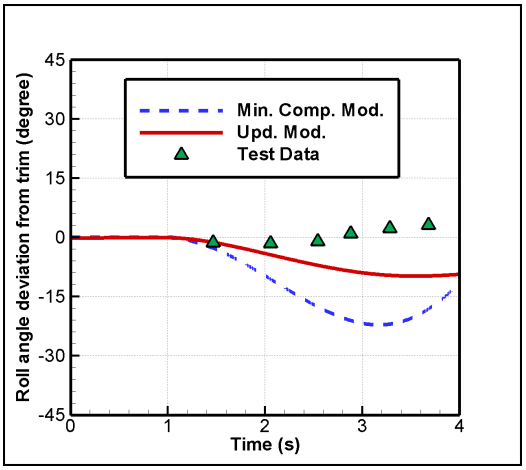

Figure 4.27: Euler roll angle response of the simulation models and test data.

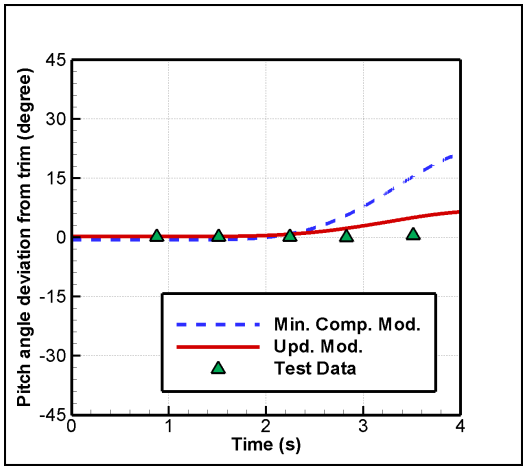

Figure 4.28: Euler pitch angle response of the simulation models and test data.

Roll and pitch Euler angle deviations of the simulation models are plotted in figures 4.27 and 4.28, respectively. The minimum complexity model diverges from the test data when Euler roll and pitch angles are considered, while the updated model is results in a better match with the test data.

4.2.2 60 Knots Forward Flight Condition

A step input of one inch is applied to pilot controls of the simulation models. All simulations start initially from a trimmed 60 knots forward flight condition. Responses are compared with the existing flight test data.

4.2.2.1 Pilot Collective Step Input

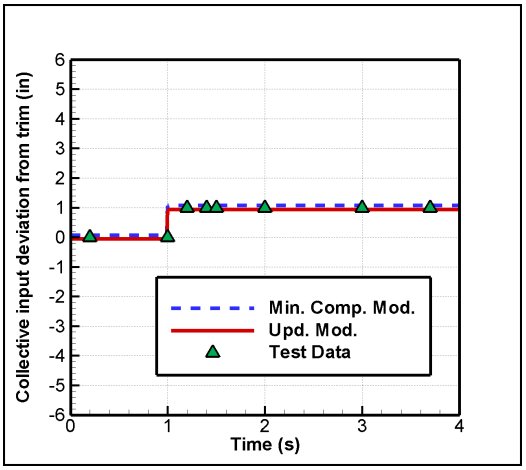

Figure 4.29: A step input of one inch pilot collective after one second of trimmed flight.

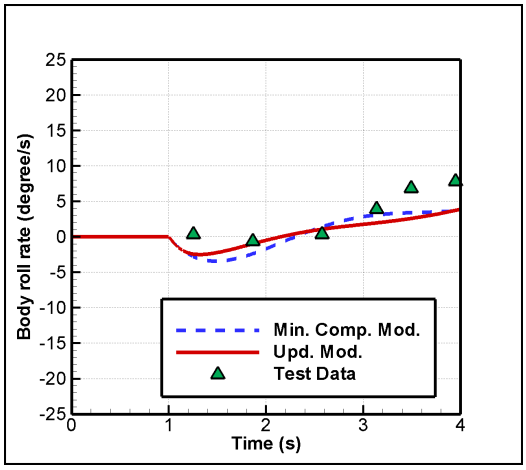

Figure 4.30: Roll rate response of the simulation models and test data.

Both the minimum complexity and the updated simulation models are subjected to an one inch step input on the pilot collective lever, shown in figure 4.29. Figure 4.30 presents the roll rate response of the simulation models and flight test. The figures show a good match between the models and the test data.

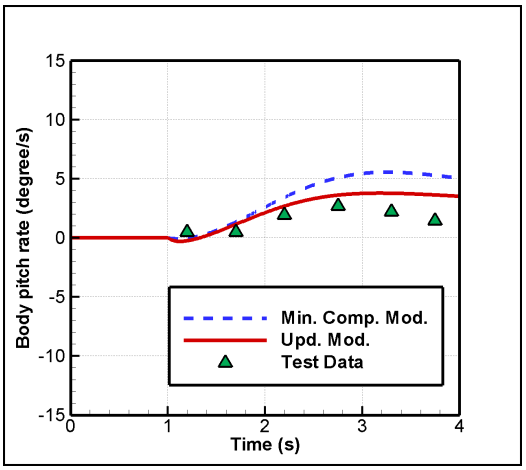

Figure 4.31: Pitch rate response of the simulation models and test data.

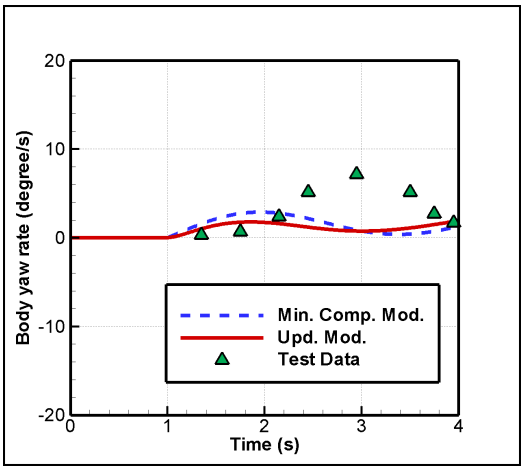

Figure 4.32: Yaw rate response of the simulation models and test data.

Figures 4.31 and 4.31 are the plots of pitch and yaw rates respectively for the one inch collective input case. The updated model shows a better match with the flight test data than the minimum complexity model in the pitch rate response. However, both models have over damped responses in yaw rate. A reason could be the interaction of the tail rotor with the wake of the main rotor.

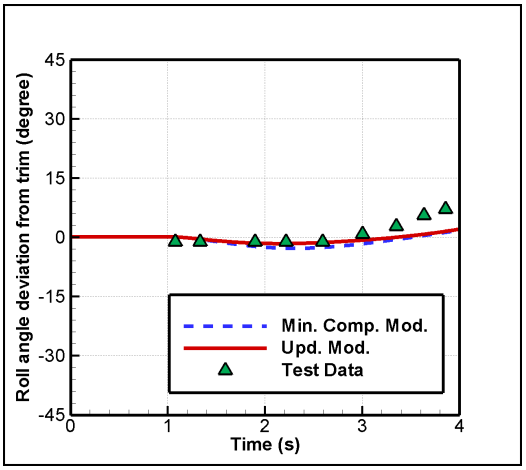

Figure 4.33: Euler roll angle response of the simulation models and test data.

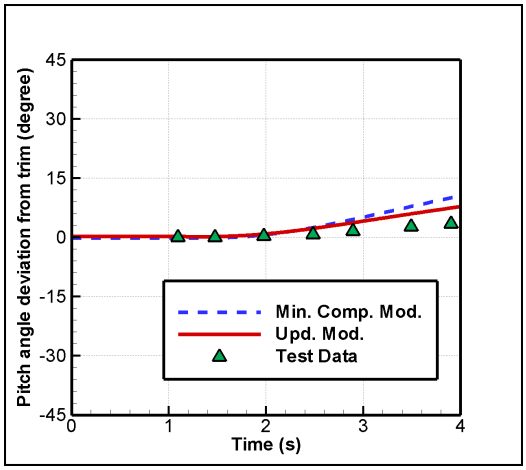

Figure 4.34: Euler pitch angle response of the simulation models and test data.

Although there are small offsets in the Euler pitch and roll angle values with the flight test data, both simulation models capture the right trend (Figures 4.33 and 4.34).

4.2.2.2 Pilot Longitudinal Cyclic Step Input

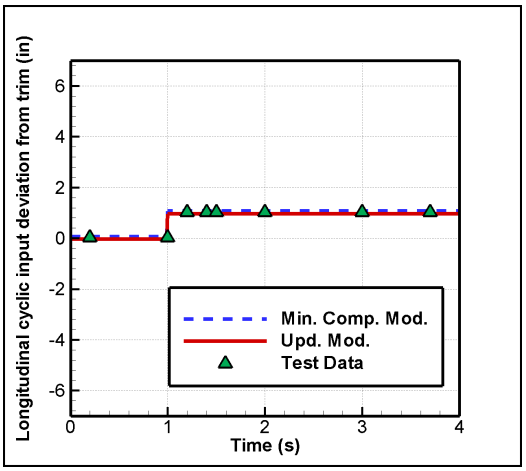

Figure 4.35: A step input of one inch pilot longitudinal cyclic after one second of trimmed flight.

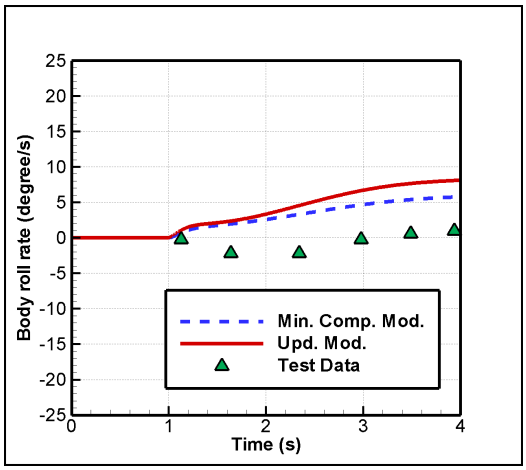

Figure 4.36: Roll rate response of the simulation models and test data.

Both models are subjected to one inch longitudinal step input after one second of trimmed flight, shown in figure 4.35. Both models have reverse body roll rate responses due to exclusion of off-axis modifications. Figure 4.36 presents the off-axis response of the simulation models in lateral channel.

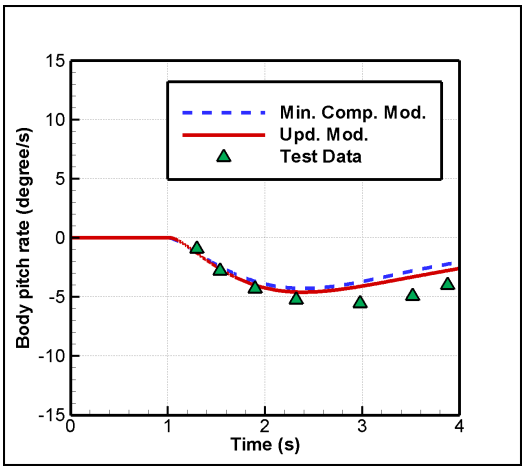

Figure 4.37: Pitch rate response of the simulation models and test data.

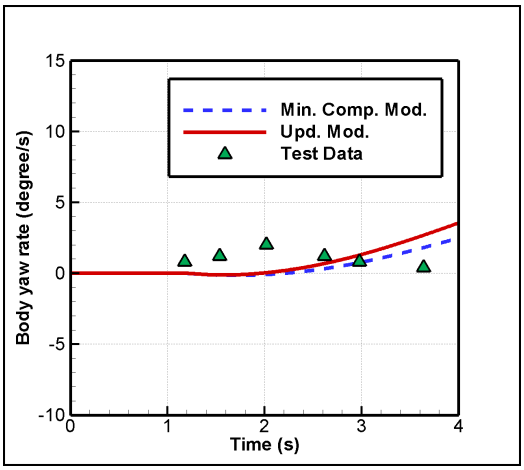

Figure 4.38: Yaw rate response of the simulation models and test data.

Figure 4.37 indicates that the primary effect of longitudinal cyclic input appears in the pitch rate responses. They are almost the same for both of the simulation models with deviation from the flight test data. However, both models have distinct yaw rate responses (figure 4.38) when compared to flight test data. A coupling effect of reverse off-axis roll response, could change the tail rotor calculations, which in turn effects the yaw rate response.

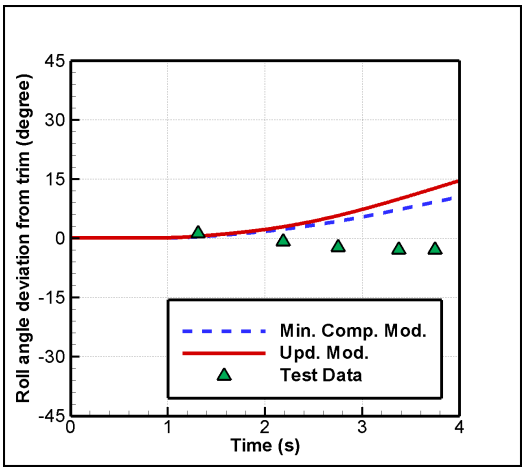

Figure 4.39: Euler roll angle response of the simulation models and test data.

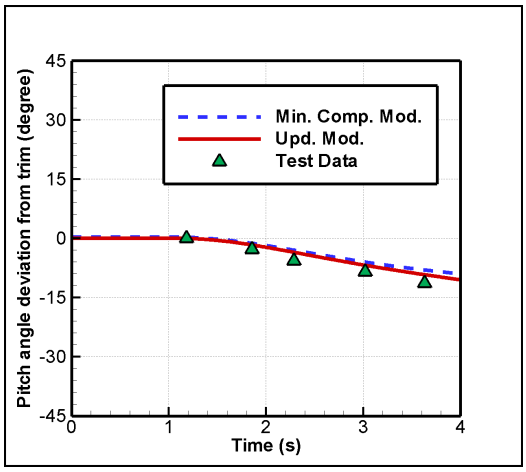

Figure 4.40: Euler pitch angle response of the simulation models and test data.

According to figure 4.39, the minimum complexity model and the updated model have different Euler roll angle responses when compared to flight test data. Both simulation models have almost the same Euler pitch angle responses with a small offset from the test data (figure 4.40).

4.2.2.3 Pilot Lateral Cyclic Step Input

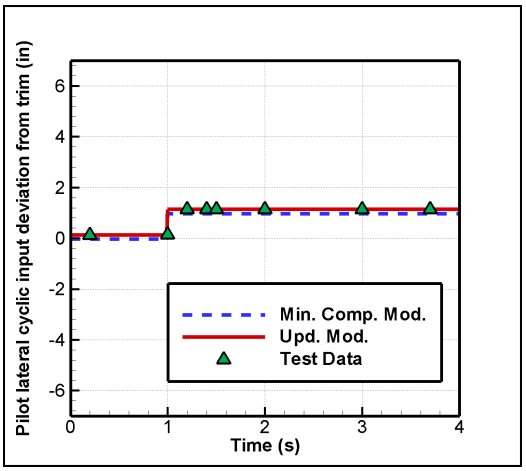

Figure 4.41: A step input of one inch pilot lateral cyclic after one second of trimmed flight.

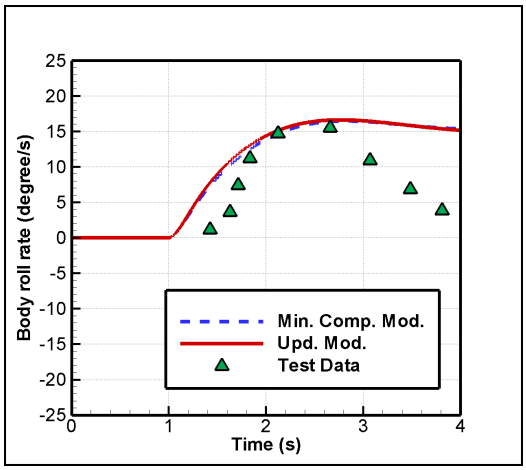

Figure 4.42: Roll rate response of the simulation models and test data.

Figure 4.41 shows the deviation of one inch pilot lateral cyclic for both models during a 60 knots forward flight condition. The updated and the minimum complexity models both have almost the same roll rate responses to the applied lateral cyclic, as plotted in figure 4.42. Models matched the initial peak values of the flight test response with small deviation. After the transient phase at about 2 seconds, both models converge to an almost fixed roll rate whereas flight test data decreases.

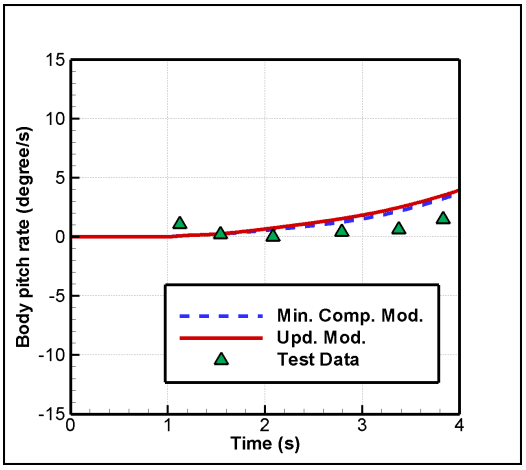

Figure 4.43: Pitch rate response of the simulation models and test data.

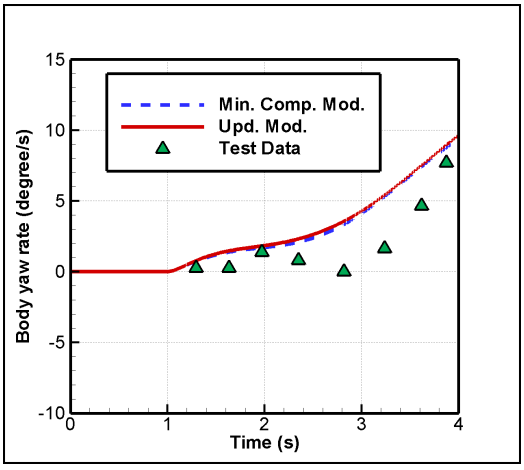

Figure 4.44: Yaw rate response of the simulation models and test data.

Figure 4.43 shows that both simulation models have same body pitch rate responses, which have the same trend of flight test data. As the figure presents, flight test data have an initial pitch rate which implies that helicopter is not trimmed during the flight test. Although there is a small initial pitch rate value, data is thought to be usable. Yaw rates of the simulation models show a damped response with the same trend of the flight test data (Figure 4.44).

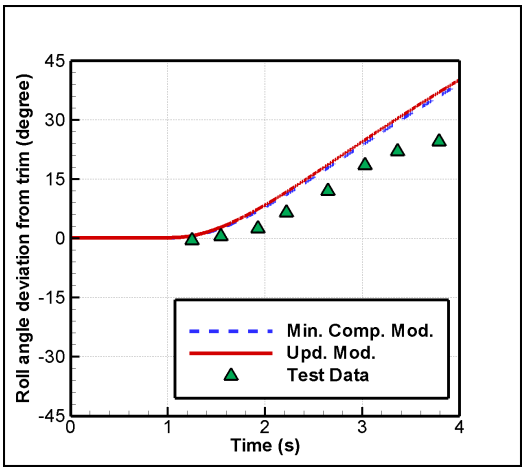

Figure 4.45: Euler roll angle response of the simulation models and test data.

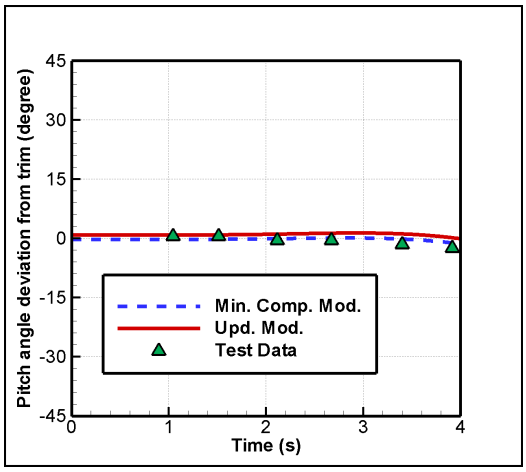

Figure 4.46: Euler pitch angle response of the simulation models and test data.

Figures 4.45 and 4.46 are plotted to observe the deviations of Euler angle response of the simulation models and test data. Both models have the same Euler angle responses with a small offset from the flight test data but pitch angle responses show a better coincidence.

4.2.2.4 Pilot Pedal Step Input

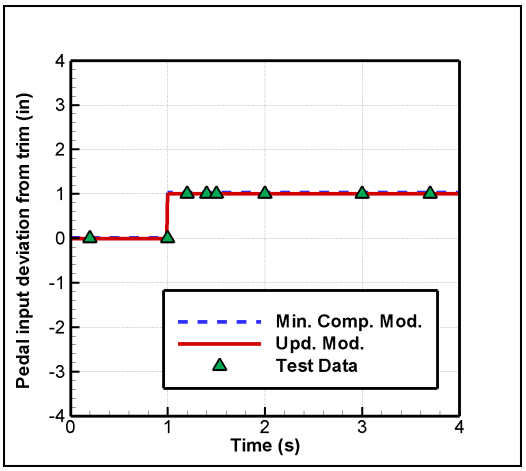

Figure 4.47: A step input of one inch pilot pedal after one second of trimmed flight.

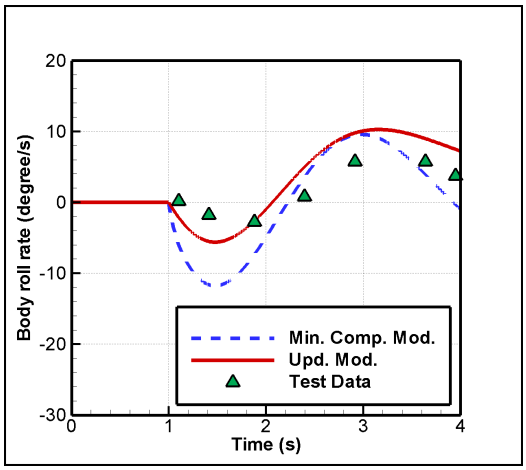

Figure 4.48: Roll rate response of the simulation models and test data.

A pilot pedal step input is applied to both models as plotted in figure 4.47 after one seconds of trimmed 60 knots forward flight. Roll rate responses are plotted in figure 4.48. The minimum complexity model has a less damped response than the updated model, which matches better to the flight test data.

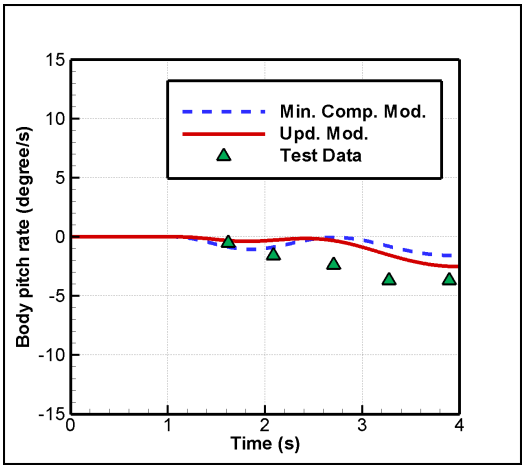

Figure 4.49: Pitch rate response of the simulation models and test data.

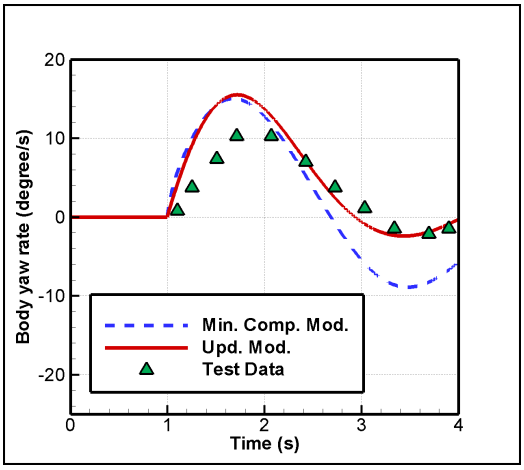

Figure 4.50: Yaw rate response of the simulation models and test data.

The pitch rate response of the simulation models are under predicted when compared to flight the test data (Figure 4.49). As a primary response of the helicopter to pedal input, the yaw rate response shows that the updated model has a better match than the minimum complexity model to the flight test data (figure 4.50).

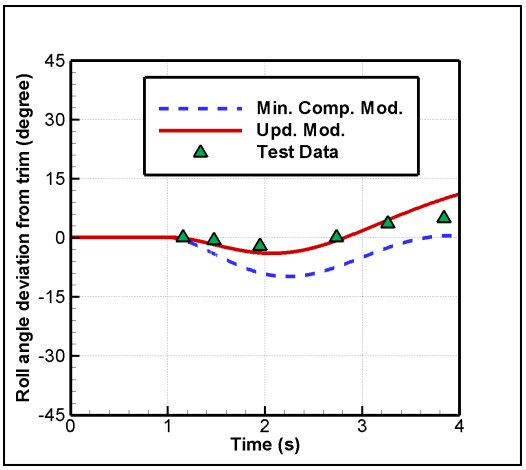

Figure 4.51: Euler roll angle response of the simulation models and test data.

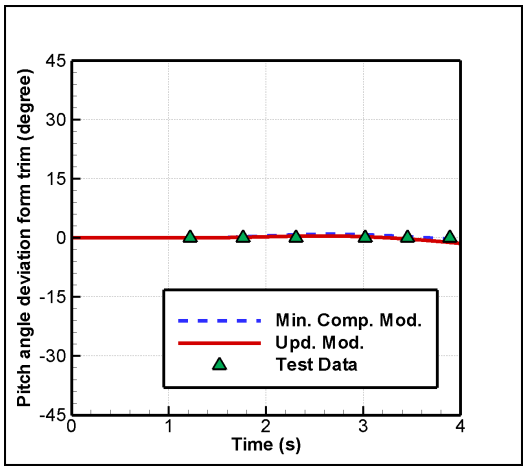

Figure 4.52: Euler pitch angle response of the simulation models and test data.

The roll angle deviation from trim of the updated model is closer to the flight test data. (figure 4.51). The pitch angle deviation responses are about the same for both models and the flight test data, as seen in figure 4.52.

4.3 Pilot Evaluation in Real Time Simulation

4.3.1 Integration Into a Simulation Environment

An important aspect of this research is to be able to integrate the mathematical model to a simulation platform. Therefore, the code is written in the C++ computer language and an object oriented approach is used. The modularity is necessary for easy modification of the various components. The codes are integrated into the open source simulation environment, Flight Gear, version 0.9.11. The Flight Gear simulation code provides a real-time simulation environment along with a visual library. More information on this tool can be found in

reference [11]. The operating system Pardus version 2007.2 RC [2.6.18-86] is used.

The Flight Gear environment allows the modeling of many detailed visual cues. Graphics of the three dimensional (3D) UH-1H helicopter model along with a cockpit design with indicators and gauges are established using graphic libraries. Animations of main rotor rotation as a function of rotor RPM, pilot control stick and pedal deflections in cockpit view, horizontal tail deflections with the related longitudinal cyclic input are some of the additional pilot cues modeled. The landing gear forces and moments are combined with the height above terrain (HAT) information form the simulation environment, enabling the helicopter to land on objects defined in the terrain data. For example, the model can be started on airport ground and can land on a hill. Some screen shots of the simulation environment are shown in figure 4.53.

Figure 4.53: Screen shots of the flying simulation models in the visual environment of Flight Gear.

4.3.2 Pilot Evaluation

Simulation models were prepared to be tested in the representative simulation environment for pilot evaluation. Commercial helicopter flight control joysticks and pedals were integrated to the simulation environment. UH-1H pilots, who are also experienced in flight simulators were asked to fly and compare the minimum complexity and updated simulation models. The comments on the minimum complexity model were that it was not representing the characteristics of the UH-1H helicopter at all. The aircraft did not respond to control inputs similar to the actual aircraft. Moreover, it is concluded that the minimum complexity simulation model has incongruously improper responses during some flight conditions. On the other hand, the updated model was judged to be more realistic throughout the whole flight envelope. Pilots agreed that the updated model simulates the real helicopter responses more accurately. But they also mentioned the need of an accurate engine model, actuator models and integrated avionics, which pilots use even while proceeding visual flight rules (VFR). Some photos taken during pilot evaluation are shown in figure 4.54.

Figure 4.54: Some photos taken during pilot evaluation.

CHAPTER 5

CONCLUSION

In this study, two real time mathematical helicopter simulation models with different levels of fidelity are developed, compared and tested in a representative simulation environment.

Baseline model is the minimum complexity model, which presents the idea of including as simple models as possible. It only includes the effects that a pilot would feel during a real-time simulation. The second model is the updated model, which includes advanced and more complicated modeling approaches specific to the UH-1H. The updated model represents a higher fidelity level. Both models use the component built up method. Some of the modifications of the components of the updated model are as follows: Three state Peters-He inflow model for the main rotor, extended tail rotor iteration, simplified aerodynamic based approach for the horizontal tail and updated fuselage calculations. Additional features related to the updated model are models of the ground effect, stabilizer bar, landing gears, etc. Also, some updates are provided to the calculation of the thrust coefficient, altitude effects and the inclusion of additional terms in the 6 Degree-of-Freedom (DOF) mode calculations. No study has been done on significance of each upgrade, rather the effect of the upgrades has been evaluated as a whole. It could be the topic of a future study to establish the significance of each individual upgrade.

Both models are trimmed using a flight control system for various forward flight conditions. Trimmed models are subjected to pilot step inputs of collective, pedal, longitudinal and lateral cyclic. Time domain responses to the applied pilot controls are observed and compared with existing flight test data. The updated model resulted in a more convenient response than the minimum complexity model when compared to flight test data. Generally, the updated model shows a better consistency with the test data. On the other hand, both models display the lack

of off-axis modifications and thus reverse secondary responses are observed. The weakest part of the modeling seems to be the roll response of the helicopter in low speeds. It seems that better component interaction and tail rotor models would be needed for a more realistic response.

Both models are integrated to a real time simulation environment with pilot collective, cyclic joysticks and pedals for pilot evaluation. Pilots with simulator experience tested the simulation models and they both concluded that the updated model has a considerable high realistic response to pilot inputs than the minimum complexity model throughout the flight envelope.

To sum up, verifications and evaluations indicate that a great improvement in simulation fidelity is achieved by modifying the minimum complexity model to an updated model of UH-1H helicopter. The minimum complexity approach was not enough to satisfy helicopter pilots, nor did it agree with flight test data. A decent simulation model, updated model, was obtained only after the inclusion of the various updates like Peters-He inflow model, ground effect, modified tail rotor iteration, etc.

5.1 Future Work

Suggested future works, which mainly require higher computational capabilities, are listed below;

- A detailed engine model, which covers the whole flight regime and capable of simulating the engine failures, can be included to the simulation models. Furthermore, start-up and autorotation procedures can be trained by the simulation models.
- Blade flapping dynamics can be improved with aeroelastic blade considerations.
- Peters-He inflow model can be extended to have more detailed states with higher harmonic, advanced flapping dynamics integration, ground effect, off axis and vortex ring state decent regime modifications.
- Blade section of main rotor can be adjusted to NACA0012 airfoil and more radial sections can be chosen for higher detail.
- Aerodynamic methods can be extended to include highly turbulent, compressible air

passing over fuselage, tail boom, horizontal and vertical tail surfaces.

- A detailed wind and turbulence gust models can be implemented to the simulation model.
- With an adequate engine model, fuel consumption due to variable power settings can be considered and thus, weight and center of gravity of the simulation helicopter model can be altered during the flight.
- Tail rotor calculations can be accomplished by Peters-He inflow model even with few states and interaction of the main rotor inflow can be implemented to the tail rotor calculations.
- Flight tests, particularly for simulation validations, can be performed with high precision measurement units.

REFERENCES

[1] R. K. Hefley, M. A. Mnich "*Minimum-Complexity Helicopter Simulation Math Model*", Contract NAS2-11665, Muadyne Report 83-2-3, Ames Research Center , October 1986

[2] P. D. Talbot, L. D. Corliss, "*A Mathematical Force and Moment of a UH-1H Helicopter For Flight Dynamics Simulations*", NASA TM 73-254, June 1977

[3] G. D. Padfield, M. Pavel, D. Casolaro "*Fidelity of Helicopter Real Time Simulation Models* ", 61st Annual Forum of the American Helicopter Society, Grapevine,Texas, June 2005

[4] C. H. Tho, C. S. Sparks, A. K. Sareen "*Efficient Helicopter Landing Gear Dynamic Drop Simulation Using LS-DYNA*", American Helicopter Society 59th Annual Forum, Phoenix, Arizona, May 6-8, 2003

[5] J.G. Leishman "*Principles of Helicopter Aerodynamics*", Cambridge Aerospace Series, 2000

[6] G. D. Padfield "*Helicopter Flight Dynamics: The Theory and Application of Flying Qualities and Simulation Modeling*", AIAA Education Series, 1996

[7] R. W. Prouty "*Helicopter Performance, Stability, and Control*", Krieger Publishing Company, 1995

[8] M. Mittal, J. V. R. Prasad "*Modeling the UH-1 Helicopter using the ARMCOP Program*", Interim Progress Report, Georgia Institute of Technology 1994

[9] "*Turkish Mod UH-1H Helicopter Training Simulator Acceptance Test Manual*", Volume I CH.4-30, SY3466v1, 19 June 1989

[10] "*Turkish Mod UH-1H Helicopter Training Simulator Acceptance Test Manual*", Volume II CH.31-71, SY3466v2, 19 June 1989

[11] Flight Gear website "*http://www.flightgear.org/* ", as accurate of June 2008.

[12] Bell UH-1H Helicopter Picture "*http://www.copyright-free-pictures.org.uk/ helicopters /20-bell-uh-1h.htm* ", as accurate of June 2008.

[13] Bell UH-1H Stabilizer Bar Picture "*http://www.aircav.com/img/cav/stabil001.gif*", as accurate of June 2008.

[14] R. E. Sheldahl, Klimas, P. C. "*Characteristics of Seven Airfoil Sections Through 180 Degrees Angle of Attack for Use in Aerodynamic Analysis of Vertical Axis Wind Turbines*", SAND80-2114,Sandia National Laboratories, Albuquerque, New Mexico, March 1981

[15] F. O. Smetana "*Introductory Aerodynamics and Hydrodynamics of Wings and Bodies: A Software-Based Approach* ", AIAA Education Series, 1997

[16] L. K. Henry, A. C.Cynthia , R. Y. Kenneth, B. L. Michael "*Flight Investigation the Effect of Tail Boom Strakes on Helicopter Directional Control*", AVSCOM Technical Report 93-A-003, February 1993

[17] F. Coton, J. Marshall , R. Galbraith, R . Green "*Helicopter tail rotor orthogonal blade vortex interaction*", Progress in Aerospace Sciences , Volume 40 , Issue 7 , Pages 453 - 486

[18] T. M. Fletcher, R. E. Brown "*Modeling the interaction of helicopter main rotor and tail rotor wakes*",Royal Aeronautical Journal Volume 111, Number 1124, 2007

[19] J. E. Corban, A. J. Calise, J. V. R. Prasad, G. Heynen, B. Koenig, J. Hur "*Flight Evaluation of an Adaptive Velocity Command System for Unmanned Helicopters*",AIAA Guidance, Navigation and Control Conference and Exhibit, 11-14 August 2003, Austin, Texas

[20] J. V. R. Prasad, A. J. Calise, Y. Pei, J. E. Corban, "*Adaptive Control Senthesis and Flight Test Evaluation on an Unmanned Helicopter*", IEEE International Conference on Control Applications, 1999

[21] A. J. Calise, R. T. Rysdyk "*Nonlinear Adaptive Flight Control Using Neural Networks*",IEEE Controls Systems Magazine, 1998

[22] A. J. Calise, R. T. Rysdyk "*Nonlinear Adaptive Control of Tiltrotor Aircraft Using Neural Networks*",1997 SAE/AIAA World Aviation Congress, October 14-16, 1997, Anaheim, CA.

[23] A. J. Calise, R. T. Rysdyk "*Adaptive Model Inversion Flight Control For Tiltrotor Aircraft*",AIAA Guidance,Navigation and Control Conference, Aug. 1997, Paper No: 97-3758

[24] O. Tarimci, I. Yavrucuk "*Simulation Evaluation of a Flight Control System for an Autonomous Fullsize Helicopter*",4. Ankara International Aerospace Conference, 10-12 September, 2007 - METU, Ankara Paper No: AIAC-2007-062

[25] D. Learmount "*Low-cost Simulation can Transform Helicopter Training* ",Flight International, 28 September 2007

[26] S. B. Jon "*JSBSim:An Open Source Flight Dynamics Model in C++* ",AIAA Modeling and Simulation Technologies Conference and Exhibit 16-19 August 2004, Providence, Rhode Island

[27] Anon. "*World Aircraft Accident Summary 1990-2001 Index-Cap 479* ",Civil Aviation Authority, Airclaims, 2002

[28] D. Ledar "*Helicopter Simulation for Naval Training* ",AIAA 94-3435, Thomson Training and Simulation, Gergy-Pontoise France,1994

[29] E. Russel, S. Jennie "*Helicopter trimming and tracking control using direct neural dynamic programming* ",IEEE transactions on neural networks, Vol.14, No.4, July 2003

[30] T. Wilcock, C. A. Thrope "*Flight simulation of a Wessex helicopter,a validation exercise* ",Aeronautical Research Council C.P. No. 1299, Aerodynamics Department, R.A.E., Bedford, 1974

[31] S. Sarathy, V. R. Murthy "*An Advanced Rotorcraft Flight Simulation: Parallel Implementation and Performance Analysis*",AIAA Guidance,AIAA-93-3550-CP, 1993

[32] T. N. C. Robert "*A Simplified Rotor System Mathematical Model for Piloted Flight Dynamics Simulation*",NASA Technical Memorandum 78575, NASA Ames Research Center, May 1979

[33] T. N. C. Robert "*Effects of Primary Rotor Parameters on Flapping Dynamics*",NASA Technical Paper 1431, NASA Ames Research Center, January 1980

[34] D.T. Peter, E.T. Bruce, A.D. William, T.N.C. Robert "*A Mathematical Model of a Single Main Rotor Helicopter for Piloted Simulation* ",NASA Technical Memorandum 84281, September 1982

[35] M.A. Glauert "*A General Theory of Autogyro* ",Royal Aeronautical Establishment R. and M. No. 1111, November 1926

[36] C.N.H. Lock "*Further Development of Autogyro Theory*",Royal Aeronautical Establishment R. and M. No. 1127, March 1927

[37] C. Munzinger "*Development of a Real-Time Flight Simulator for an Experimental Model Helicopter*",Diploma Thesis, Georgia Institute of Technology School of Aerospace Engineering, Atlanta, December 1998

[38] M. Pavel "*Prediction of the Necessary Degrees of Freedom for Helicopter Real-time Simulation Models*", AIAA 2005-6206, AIAA Modeling and Simulation Technologies Conference and Exhibit, San Francisco California, August 2005

[39] I. C. Cheeseman,W. E. Bennett "*The Effect of the Ground on a Helicopter Rotor in Forward Flight* ", ARC RM 3021, 1955

[40] D. M. Pitt,D. A. Peters "*Theoretical Prediction of Dynamic-Inflow Derivatives*", Vertica Vol. 5, 1981.

[41] D. M. Pitt,D. A. Peters "*Rotor Dynamic Inflow Derivatives and Time Constants from Various Inflow Models*", 9^{th} European Rotorcraft Forum Paper No:55, Italy, September 1983.

[42] R. T. N. Chen "*A Survey of Nonuniform Inflow Models for Rotorcraft Flight Dynamics and Control Applications*", NASA TM 102219, November 1989.

[43] D. A. Peters, C. J. He "*Finite-State Induced-Flow Model for Rotors in Hover and Forward Flight* ", 43^{rd} Annual National Forum of the American Helicopter Society, Boston, May 1987

[44] D. A. Peters, C. J. He, D. D. Boyd "*Correlation of Measured Induced Velocities with Finite-State Wake Model*", 45^{th} Annual National Forum of the American Helicopter Society, Boston, May 1989

[45] D. A. Peters, C. J. He "*Comparison of Measured Induced Velocities with Results from a Closed-Form Finite-State Wake Model in Forward Flight*", 45^{th} Annual National Forum of the American Helicopter Society, Boston, May 1989

[46] M. D. Takahashi "*A Flight Dynamic Helicopter Mathematical Model with a Single Flap-Lag-Torsion Main Rotor* ", NASA TM 102267, Ames Research Center California, February 1990

[47] K. R. Krothapalli, J. V. R. Prasad, D. A. Peters "*Development of a Comprehensive wake theory for lifting rotors*", AIAA-96-3390-CP, 1996

[48] H. Xin, J. V. R. Prasad, D. A. Peters "*Unsteady Aerodynamics of Helicopter Rotor Hovering in Dynamic Ground Effect* ", AIAA-98-4456 , 1998

[49] C. Theodore, R. Celi "*Helicopter Flight Dynamic Simulation with Refined Aerodynamics and Flexible Blade Modeling*", 56^{th} Annual Forum of American Helicopter Society, Virginia, May 2000

[50] J. A. Morillo, D. A. Peters "*Comparison of Exact Time Domain Solutions for Rotor Inflow Finite-State Results*", 56^{th} Annual Forum of American Helicopter Society, Virginia, May 2000

[51] J. Zhao, J. V. R. Prasad, D. A. Peters "*Simplified Dynamic Wake Distortion Model for Helicopter Translational Flight*", AIAA 2002-4400, 2002

[52] S. S. Houston, R. E. Brown "*Rotor-Wake Modeling for Simulation of Helicopter Flight Mechanics for Autorotation*", Journal of Aircraft Vol.40 No.5, September 2003

[53] K. Yu, D. A. Peters "*A Closed Form Representation of Three-Dimensional State-Space Influence Coefficients*", 61^{st} Annual Forum of American Helicopter Society, June 2005

[54] J. Zhao "*Dynamic Wake Distortion Model for Helicopter Maneuvering Flight*", Doctorate Thesis, Aerospace Engineering School of Georgia Institute of Technology, March 2005

[55] J. F. Horn, D. O. Bridges, D. A. Washspress, S. L. Rani "*Implementation of a Free-Vortex Wake Model in Real Time Simulation of Rotorcraft* ", Journal of Aerospace Computing, Information and Communication Vol.3, March 2006

[56] C. Chen "*Development of a Simplified Inflow Model for a Helicopter Rotor in Descent Flight*",Doctorate Thesis, Aerospace Engineering School of Georgia Institute of Technology, August 2006

[57] V. R. M. Hoydonck "*Literature Survey on the Simulation and Handling Qualities for Helicopters Operating Near Ship Decks* ", May 2006

[58] D. L. Key, R. S. Hanson, W. B. Cleveland, W. Y. Abbot "*Helicopter Simulation Validation Using Flight Data* ", NASA Technical Memorandum 84291, November 1982

[59] A. J. Rehmann "*A Handbook of Flight Simulation Fidelity Requirements for Human Factors Research*", DOT/FAA/CT-TN95/46, December 1995

[60] J. Zhao "*Dynamic Wake Distortion Model for Helicopter Maneuvering Flight*", Doctor of Philosophy Thesis, Georgia Institute of Technology, March 2005

Appendix A

GEOMETRY SPECIFICATIONS OF THE UH-1H HELICOPTER

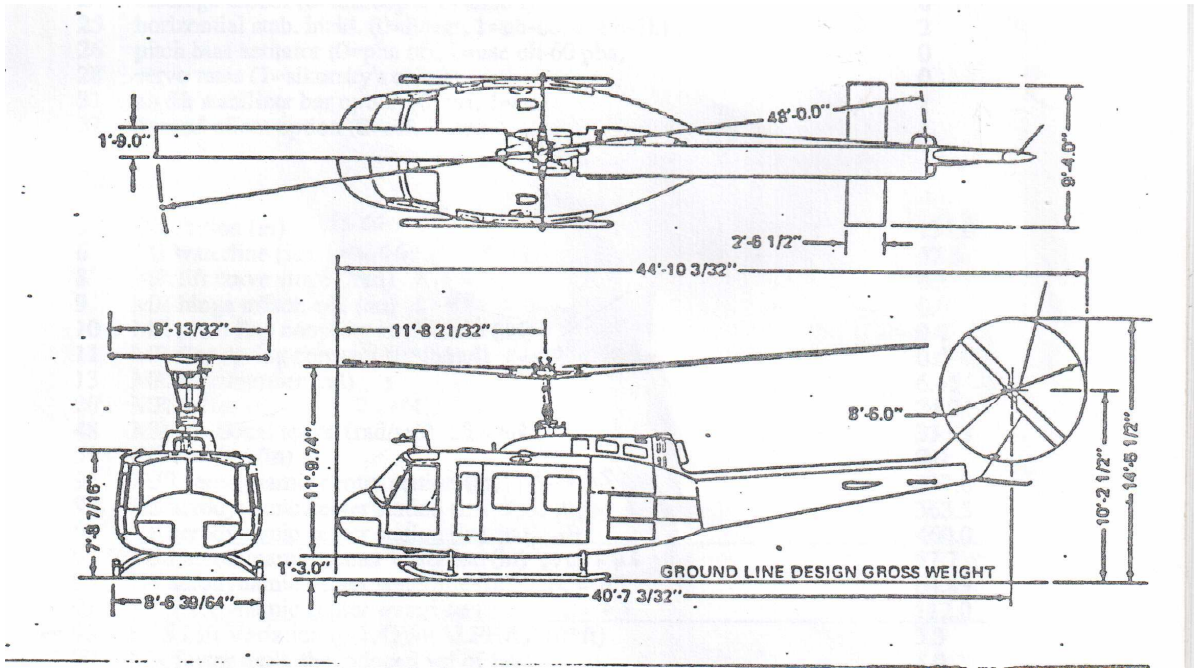

Figure A.1: Geometric sketch of UH-1H [8]

Table A.1: Summary of UH-1H Physical Constraints [2]

Main Rotor		
	Radius	24.13 ft
	Chord	1.75 ft
	Tip Speed (ΩR)	760 ft/s
	Hub stationline	133.5
	Hub waterline	136.5
	Solidity	0.046
Tail Rotor		
	Radius	4.25 ft
	Chord	0.70 ft
	Tip Speed (ΩR)	740 ft/s
	Hub stationline	479.4
	Hub waterline	137.5
	Solidity	0.105
Center of Gravity		
	Stationline	130
	Waterline	55
Horizontal Stabilizer		
	Area	16.4 ft^2
	Span	8.75 ft
	1/4 c station	380
Vertical Fin		
	Area	12 ft^2
	Span	4.5 ft
	1/4 c station	460
	a.c., waterline	112
Fuselage		
	fe_l	19.2 ft^2
	C_{L_α} (includes stab.)	0.036/deg
	C_{m_α} (includes stab.)	0
	S_ref	48 ft^2
	l_ref	39 ft
	Mast tilt	+5 deg fwd.
Control Travels (full throw)		
	Collective stick	11 in.
	Longitudinal stick	12.9 in.
	Lateral stick	12.6 in.
	Pedal	6.9 in.

Appendix B

MAIN ROTOR INFLOW DISTRIBUTIONS

In this appendix, Peters-He inflow model results are provided for the main rotor of the updated model. Here, local induced velocity, thrust coefficient and angle of attack values are calculated instantaneously for each blade. Therefore, distributions of these variables are obtained for per revolution of the main rotor. During the calculations, effects of blade flapping rates and fuselage on inflow distribution are ignored in the inflow computations. Following graphs are plotted to present the inflow, angle of attack and thrust distributions after an applied pilot control to the trimmed helicopter model for a chosen flight condition. To illustrate the case, firstly, updated model is trimmed to 60 knots forward flight condition, as done in chapter 4. Secondly, one inch pilot input in lateral or longitudinal channels is applied separately at the first second of the trimmed flight. As presented in chapter 4, corresponding angular rate responses of the helicopter to the applied pilot controls are shown in sections B.1 and B.2. Moreover, it is worth to mention that translational accelerations also have to be considered even though not plotted. Finally, time history of the distributions are obtained. Since the rotor is not isolated from the helicopter body, it is thought to be improper to compare results with existing wind tunnel experiments.

B.1 Longitudinal Step Input to 60 Knots Trimmed Flight

Rate response graphs in chapter 4 are re plotted to show the responses of the updated simulation model. Model is initially trimmed to 60 knots forward flight and subjected to a longitudinal step input after first second. In each distribution graph, instant time of the distribution is presented. To understand the instant distribution of the helicopter, one must also consider rotational rate responses of the helicopter for the mentioned particular time. For each graph, the distribution with t=0s, is the trimmed one. In addition, the distribution with t=1s is the one just after the applied longitudinal control. Applied longitudinal control is presented in

figure B.1 and angular rates are shown in figures B.2, B.3 and B.4.

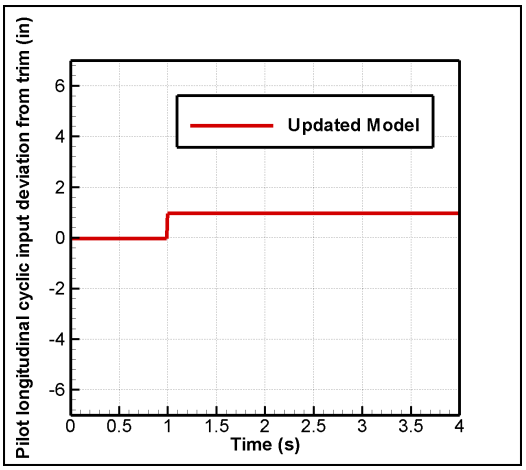

Figure B.1: A step input of one inch pilot longitudinal cyclic after one second of trimmed flight.

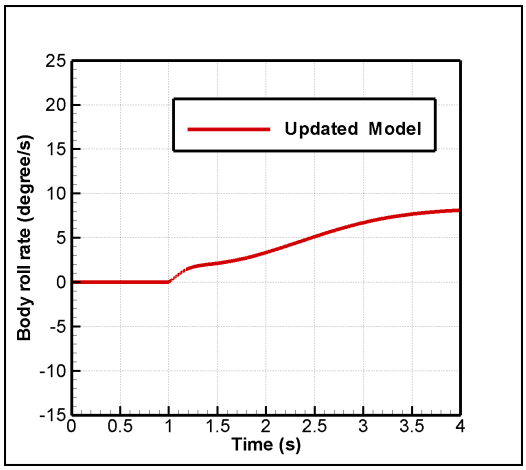

Figure B.2: Roll rate response of the updated simulation model.

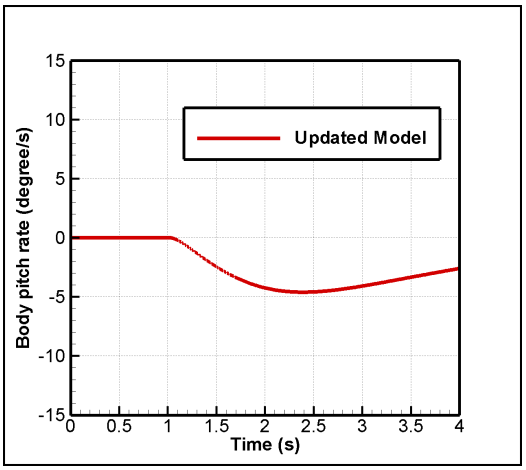

Figure B.3: Pitch rate response of the updated simulation model.

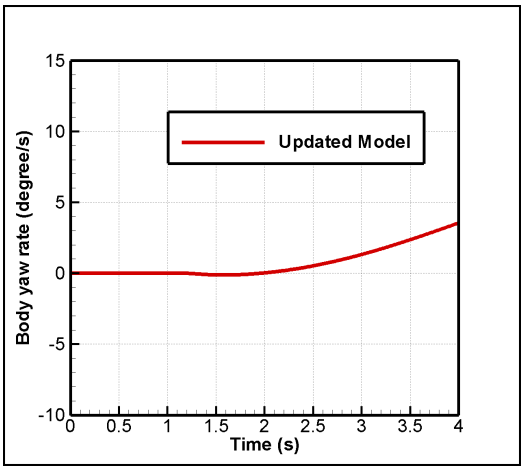

Figure B.4: Yaw rate response of the updated simulation model.

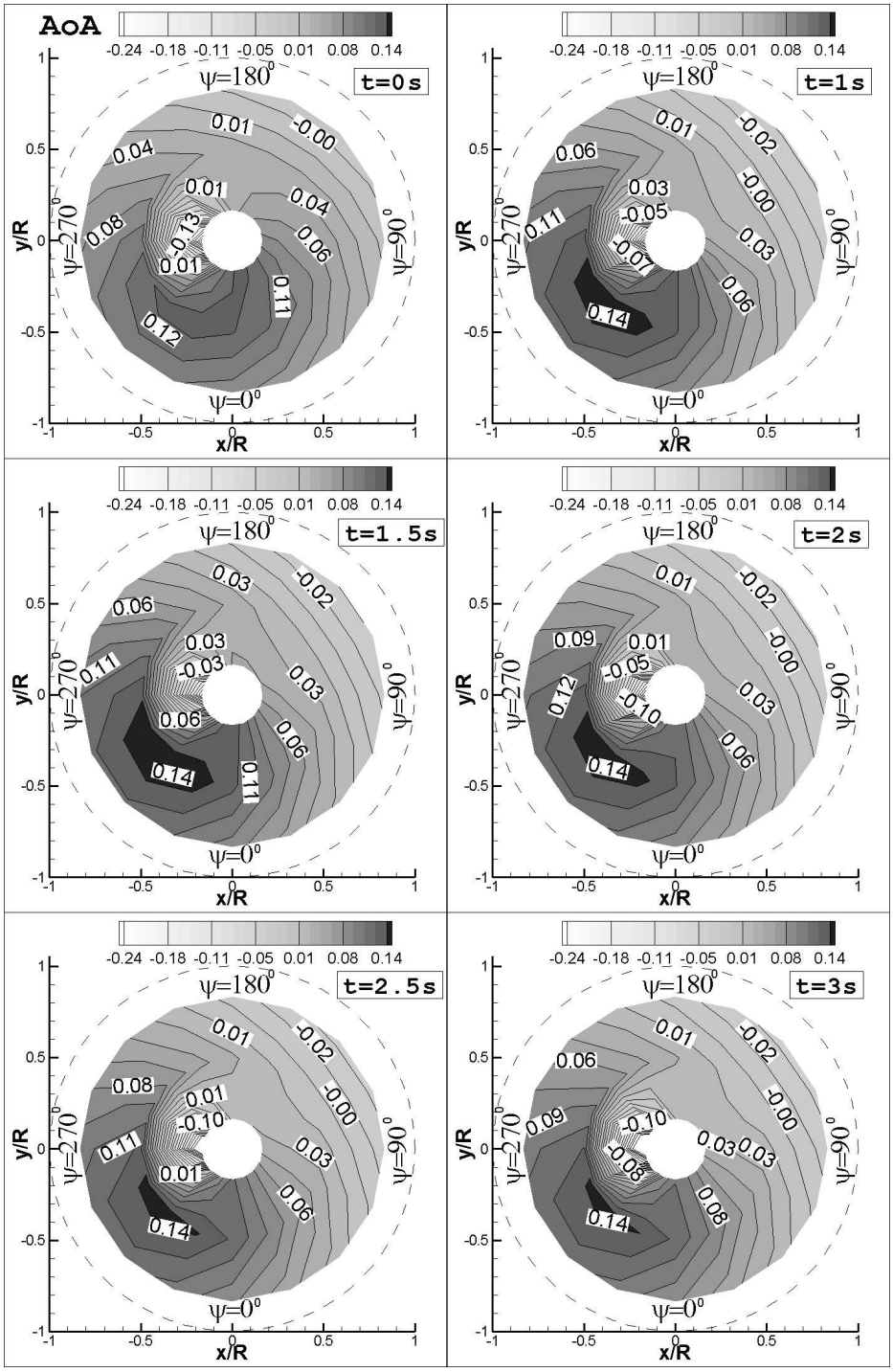

Figure B.5: Angle of attack (AoA) (rad) distribution after applied one inch longitudinal cyclic input to a trimmed 60 knots flight.

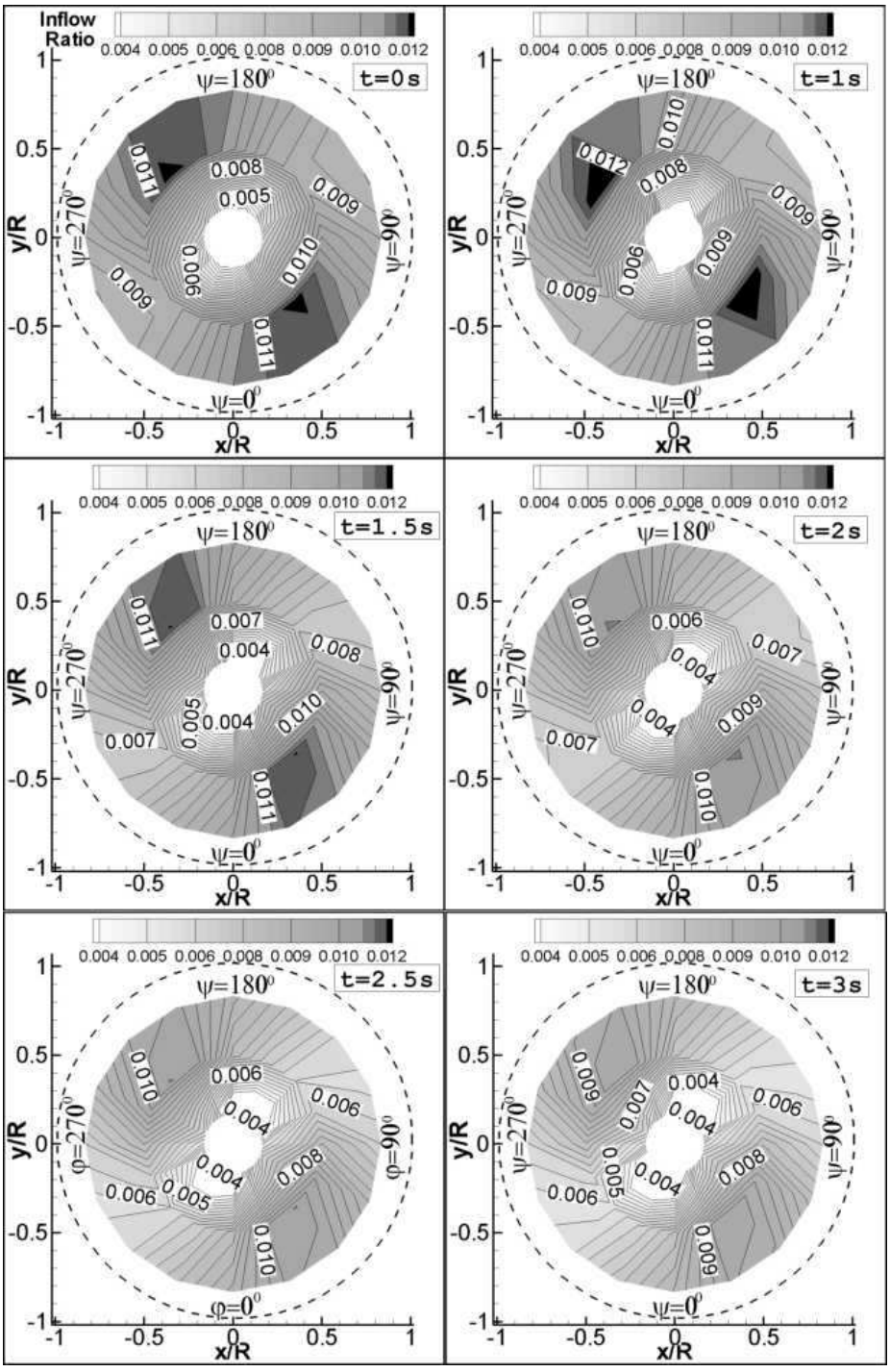

Figure B.6: Inflow ratio $V_{induced}/V_{tip}$ distribution after applied one inch longitudinal cyclic input to a trimmed 60 knots flight.

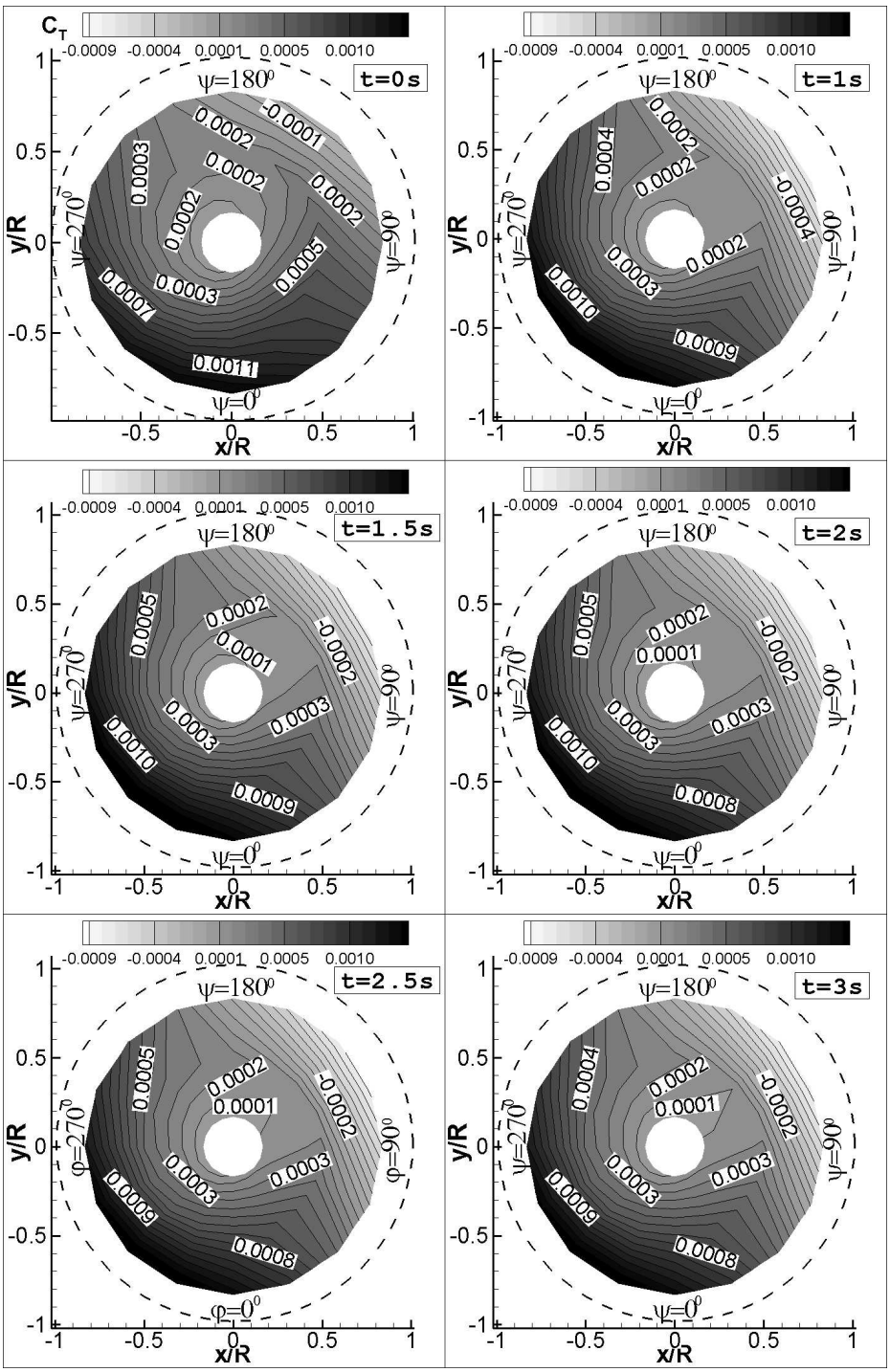

Figure B.7: Thrust ratio C_T distribution after applied one inch longitudinal cyclic input to a trimmed 60 knots flight.

B.2 Lateral Step Input to 60 Knots Trimmed Flight

Rate response graphs, as in chapter 4, are presented again to show the responses of the updated simulation model. An one inch lateral cyclic input is applied at first second of initially trimmed 60 knots forward flight condition. In each distribution graph, instant time of the distribution is presented. Applied lateral cyclic control on trim value is presented in figure B.8 and angular rates are shown in figures B.9, B.10 and B.11.

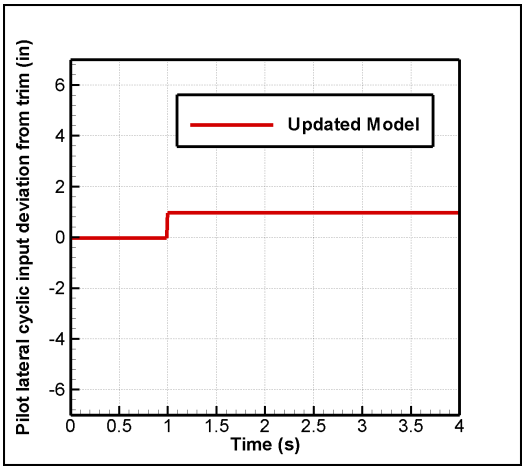

Figure B.8: A step input of one inch pilot longitudinal cyclic after one second of trimmed flight.

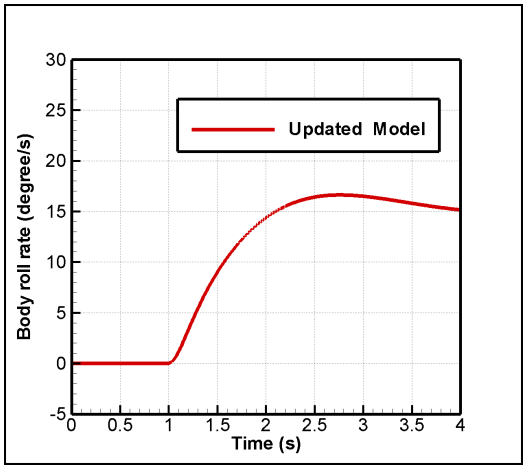

Figure B.9: Roll rate response of the updated simulation model.

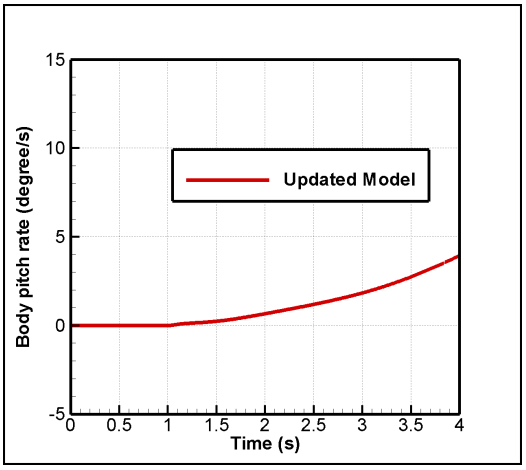

Figure B.10: Pitch rate response of the updated simulation model.

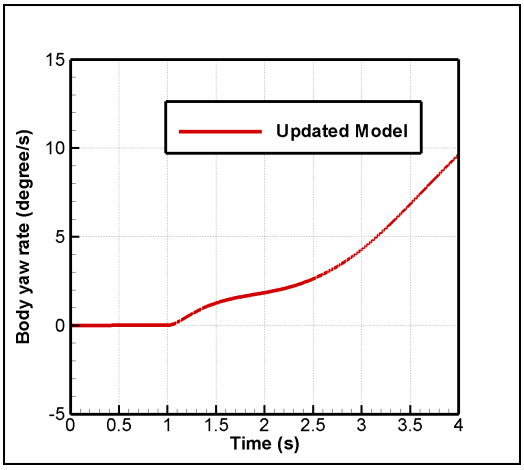

Figure B.11: Yaw rate response of the updated simulation model.

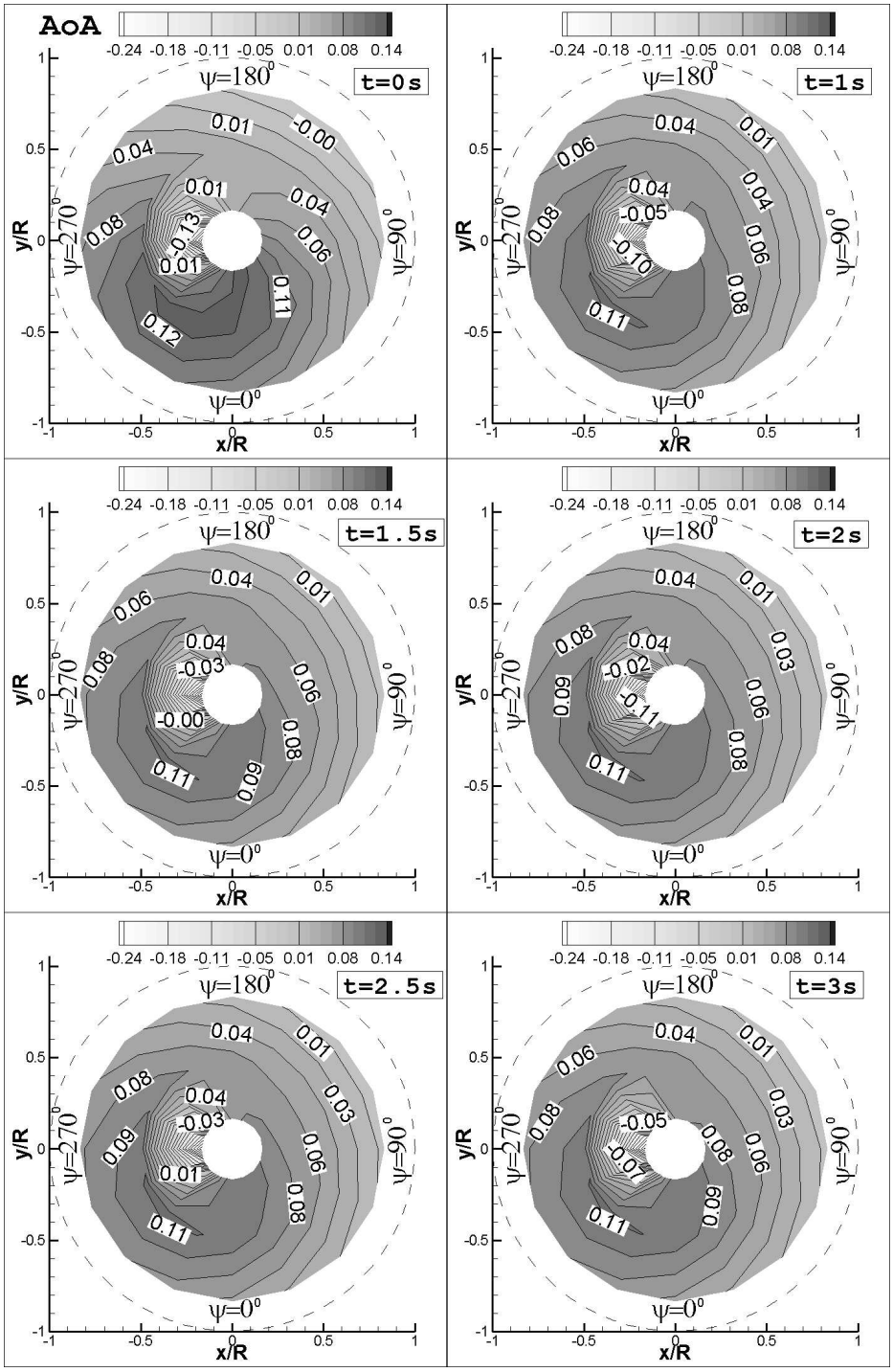

Figure B.12: Angle of attack (AoA) (rad) distribution after applied one inch lateral cyclic input to a trimmed 60 knots flight.

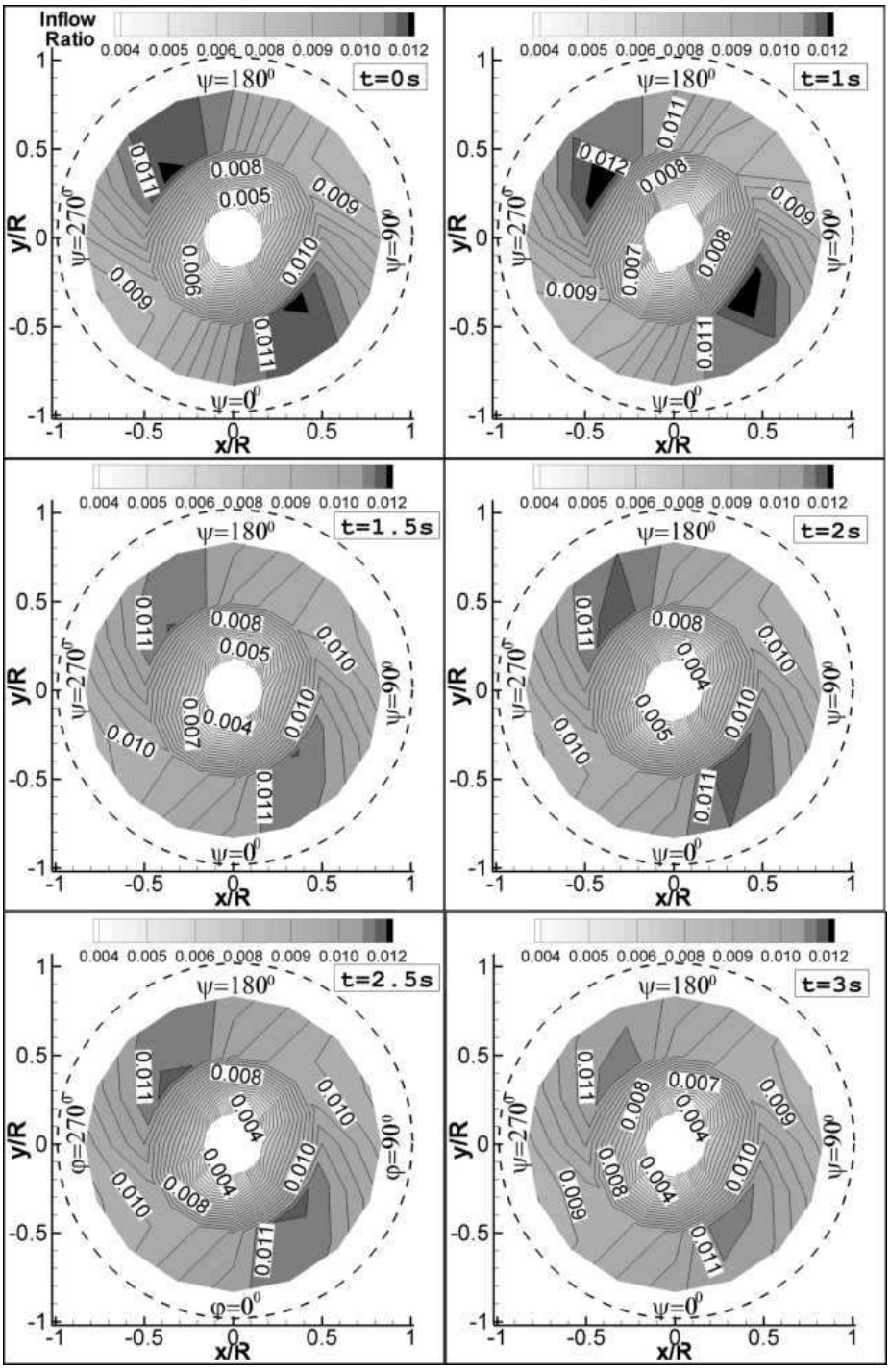

Figure B.13: Inflow ratio $V_{induced}/V_{tip}$ distribution after applied one inch lateral cyclic input to a trimmed 60 knots flight.

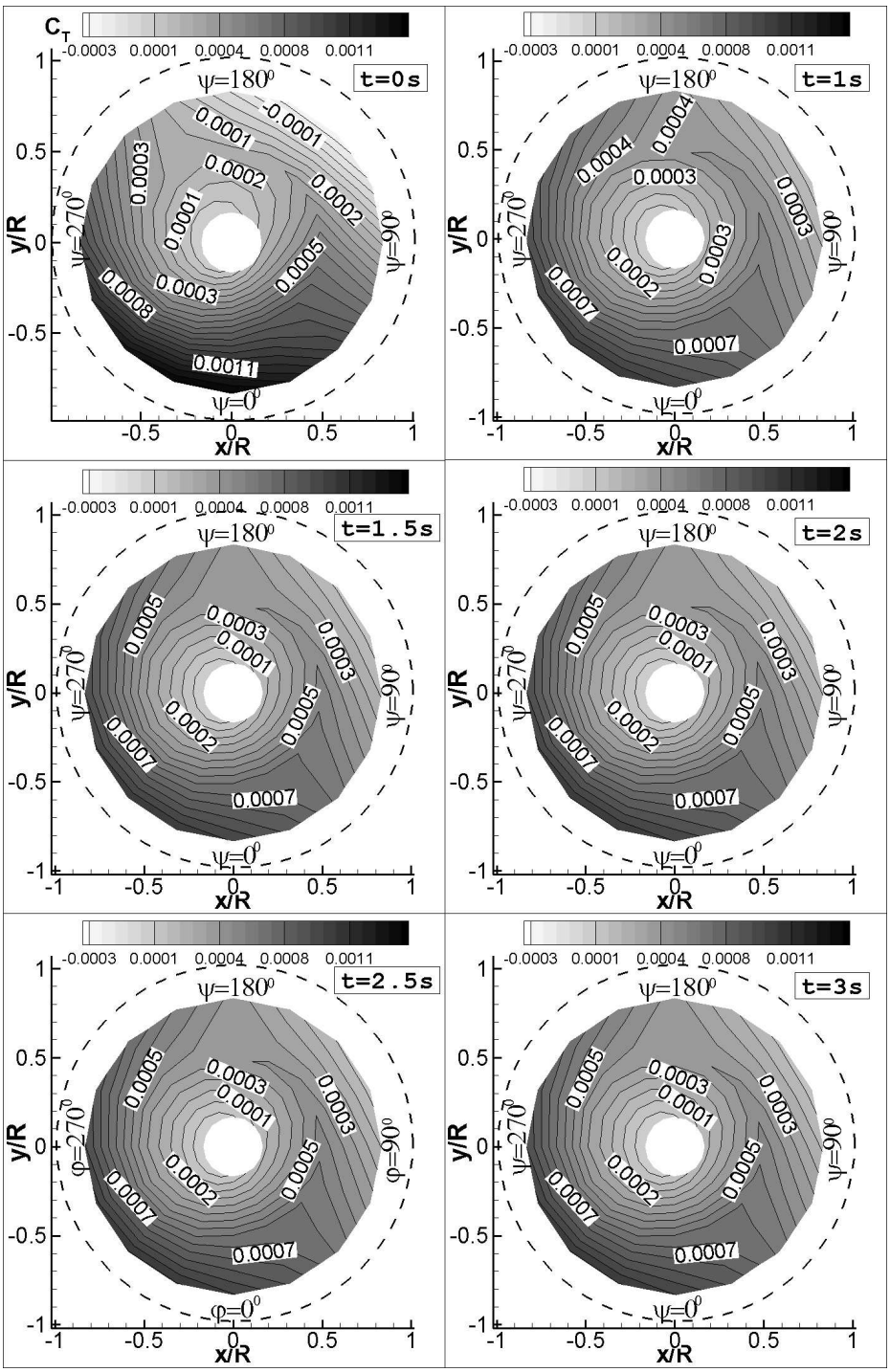

Figure B.14: Thrust ratio C_T distribution after applied one inch lateral cyclic input to a trimmed 60 knots flight.